Supplementary Information

Enhanced εr/LD and improved acceptor crystal growth enable all-polymer solar cells with outstanding efficiency, stability, and processability from a chlorinated-dimer diluent additive

Zhiyi Chen[1#], Shanhua Zhang[1#], Rui Sun[1,5*], Le Mei[2,3], Wenyan Yang[4], Zicheng Xing[1], Xinrong Yang[1*], Bo Xiao[1], Xiaohei Wu[1], Xian-Kai Chen[2,3] and Jie Min[1*]

[1]The Institute for Advanced Studies, Wuhan University, Wuhan 430072, China
E-mail: sun.rui@whu.edu.cn; yangxr@whu.edu.cn; min.jie@whu.edu.cn

[2]Institute of Functional Nano & Soft Materials (FUNSOM), Soochow University, Suzhou 215123, China

[3]State Key Laboratory of Bioinspired interfacial Materials Science, Soochow University, Suzhou 215123, China

[4]Cavendish Laboratory, Department of Physics, University of Cambridge, Cambridge, UK

[5]Anhui Province Key Laboratory for Control and Application of Optoelectronic Information Materials, Anhui Normal University, Wuhu 241002, China

[#]These authors contributed equally to this work

1. Experimental Section

Materials

Materials: PM6 purchased from Hyper PV Technology. Co., Ltd. PYT synthesized by our group as in previous works. D-SeV-Cl was synthesized as the following section. Chloroform was distilled from CaH_2 before use. 2-methoxynaphthalene (2-MN) was purchased from Aladdin. Other reagents used were purchased from commercial sources and used as received.

The catalyst $Pd_2(dba)_3$ was purchased from J&K Chemical. Chloroform was distilled from CaH_2 before use. Other reagents used were purchased from commercial sources and used as received. Compound I was synthesized according to the procedures outlined in the literature.[1] The synthetic route of D-SeV-Cl was shown in **Scheme S1.** ^{1}HNMR spectra were measured on Bruker AVANCE 600 MHz with *d-chloroform* as the solvent. The chemical shifts were reported as δ values (ppm) relative to an internal tetramethylsilane (TMS) standard. Mass spectra (MALDI-TOF-MS) were determined using an AB SCIEX 5800 Mass Spectrometer.

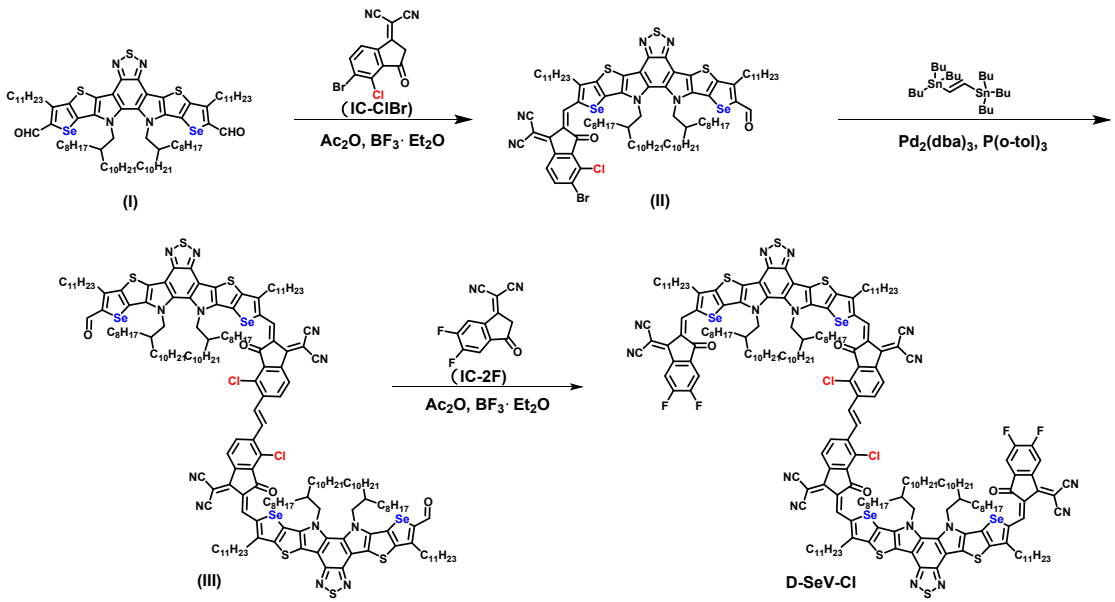

Scheme S1. The overall synthetic route to D-SeV-Cl.

Synthesis of compound II. Under the protection of nitrogen, compound I (100.0 mg, 0.068 mmol), compound IC-BrCl (21.1 mg, 0.068 mmol), acetic anhydride (0.1 mL) and dry toluene (5 mL) were added to a 25 mL two-necked round-bottom flask. Then $BF_3{\cdot}Et_2O$ (0.5 mL) was added dropwise to the mixture solution at room temperature. After 30 minutes, the reaction mixture was precipitated in methanol (100 mL). The precipitate was purified by column chromatography on silica gel with petroleum ether/chloroform (*v*/*v*=1/2) as eluent to afford compound II. (65 mg, 54%).

^{1}H NMR (600 MHz, Chloroform-d) δ 10.06 (s, 1H), 9.29 (s, 1H), 8.50 (d, J = 8.3 Hz, 1H), 7.96 (d, J = 8.3 Hz, 1H), 4.69 (d, J = 7.8 Hz, 2H), 4.62 (d, J = 7.8 Hz, 2H), 3.24 (t, J = 8.1 Hz, 2H), 3.19 (t, J = 7.8 Hz, 2H), 2.14 -2.06 (m, 2H), 1.95 -1.91 (m, 2H), 1.89 -1.82 (m, 2H), 1.54 - 1.48 (m, 4H), 1.38 (d, J = 10.2 Hz, 4H), 1.28 - 0.92 (m, 76H), 0.90 - 0.77 (m, 30H).

Synthesis of compound III. The compound II (65 mg, 0.0371 mmol), (E)-1,2-bis(tributylstannyl)ethene (9.0 mg, 0.015 mmol), $Pd_2(dba)_3$ (1.7 mg, 1.5 μmol), and P(*o*-tol)$_3$ (4.6 mg, 0.015 mmol) were added into 50 mL two-necked round bottom flask and dissolved in toluene (20 mL). The flask was purged with nitrogen and sealed under nitrogen flow. The resulting mixture was stirred and heated to reflux overnight. After cooling to room temperature, the mixture solution was poured into methanol (50 mL). The precipitate is directly used in the next reaction step after drying without further purification.

Synthesis of compound D-SeV-Cl. Under the protection of nitrogen, compound III (35.0mg, 0.010 mmol), compound IC-2F (7.2 mg, 0.031 mmol), acetic anhydride (0.1 mL), and dry toluene (5 mL) were added to a 25 mL two-necked round-bottom flask. Then $BF_3{\cdot}Et_2O$ (0.5 mL) was added dropwise to the mixture solution at room temperature. After 30 minutes, the reaction mixture was precipitated in methanol (50 mL). The precipitate was purified by column chromatography on silica gel with petroleum ether/chloroform (*v*/*v*=1/1) as eluent to afford D-SeV-Cl (25 mg, 63%).

^{1}H NMR (600 MHz, Chloroform-*d*) δ 9.28 (s, 2H), 9.19 (s, 2H), 8.74 (s, 2H), 8.57 (t, *J* = 6.9 Hz, 2H), 8.14 (s, 2H), 7.81 (s, 2H), 7.70 (t, *J* = 7.3 Hz, 2H), 4.87 – 4.67 (m, 8H), 3.30 – 3.21 (m, 4H), 3.18 – 3.04 (m, 4H), 2.26 – 2.17 (m, 4H), 1.94 – 1.85 (m, 4H), 1.69 – 0.40 (m, 232H).

MALDI-TOF MS (m/z): calcd for $C_{214}H_{270}Cl_2F_4N_{16}O_4S_6Se_4$: 3785.57 Found: 3785.24.

Nuclear magnetic resonance (NMR): ^{1}H NMR spectrum was recorded on a Bruker AVANCE NEO 600 MHz spectrometer with *d-chloroform* as the solvent. The chemical shifts were reported as δ values (ppm) relative to an internal tetramethylsilane (TMS) standard.

Matrix-assisted laser desorption/ionization time-of-flight (MALDI-TOF) Mass: MALDI-TOF mass spectra were determined using an AB SCIEX 5800 Mass Spectrometer.

***Electrochemical characterizations*:** Electrochemical properties were studied by cyclic voltammetry (CV), which was performed on a CS350H electrochemical workstation with a three-electrode system in a 0.1 M Bu_4NPF_6 acetonitrile solution at a scan rate of 100 mV/s. A glassy carbon disc coated with a sample film was used as the working electrode. A Pt wire was used as the counter electrode, and Ag/AgCl was used as the reference electrode. The HOMO/LUMO energy levels (E_{HOMO}/E_{LUMO}) can be calculated from onset oxidation/reduction potentials (ϕox/ϕred) in the cyclic voltammograms according to the equations of E_{HOMO}/E_{LUMO} =-e(ϕ_{OX}/ ϕ_{Red} +4.8-ϕ_{Fe/Fe^+}) (eV) (eV), where ϕ_{Fe/Fc^+} is the redox potential of ferrocene/ferrocenium (Fe/Fc^+) couple in the electrochemical measurement system, and the energy level of Fe/Fc^+ was taken as 4.8 eV below vacuum.

Ultraviolet-visible-near-IR spectroscopy measurements: UV-vis absorption was measured using a PerkinElmer Lambda 1050 Spectrometer.

Space charge limited current (SCLC) measurements: Single carrier devices were fabricated and the dark current-voltage characteristics were measured and analyzed in the space charge limited (SCL) regime following the references. For the electron-only devices, the structure was Glass/ITO/ZnO/Active layer/PNDIT-F3N/Ag (100 nm), where the Ag was evaporated.

The grazing incidence X-ray scattering (GIWAXS) measurement: The grazing incidence X-ray scattering (GIWAXS) measurement was carried out with a Xeuss 2.0 SAXS/WAXS laboratory beamline using a Cu X-ray source (8.05 keV, 1.54 Å) and a Pilatus3R 300K detector. The incident angle was 0.13°. The samples for GIWAXS measurements were *fabricated on silicon substrates.*

In situ Ultraviolet-visible (in-situ UV) absorption spectra measurement: For in-situ absorption spectra, an HL-2000 from Ocean Optics was used as the VIS-NIR light source, and a QE65PRO with a high-performance spectrometer from Ocean Optics was used as a detector. The characterization was through the transmission mode. The minimum integration time was 8 ms with automatically recorded spectra every 50 ms.

***Atomic Force Microscopy (AFM) measurements*:** AFM images of the thin films were obtained on a NanoscopeIIIa AFM (Digital Instruments) operating platform in tapping mode.

***Transmission electron microscopy (TEM) measurements*:** TEM measurements were carried out using a 200 kV (JEOL ARM-200F). Samples for TEM were prepared on a Cu mesh grid.

Device fabrication and testing: Solar cell devices fabrication: The solar cell devices were fabricated with a structure of Glass/ITO-Cl/Active layer/PNDIT-F3N/Ag. Pre-patterned ITO-coated glass substrates (purchased from South China Science & Technology Company Limited, the sheet resistance of the ITO glass was about 10) were washed with methylbenzene, deionized water, acetone, and isopropyl alcohol in an ultrasonic bath for 15 minutes each. After blow-drying by high-purity nitrogen, all ITO substrates are cleaned in the ultraviolet ozone cleaning system for 15 minutes. All the cleaned ITO glass is then placed in the UV-Ozone cleaning instrument using ultraviolet ozone light irradiation for 15 minutes to obtain the UV-Ozone-treated ITO anode. Afterward, the ITO surface was covered with a mixed solution of ODCB and 30% hydrogen peroxide (Sigma-Aldrich) with different volume ratios (15:2) in a Pyrex Petri dish under UV treatment for 5 minutes. After cleaning the surface of the ITO glass, UV-ozone treatment is applied for 15 minutes to obtain the surface-halogenated ITO anode. The active layers were blade-coated at 2.1 m min^{-1} to 30 m min^{-1} from toluene solution: the donor/acceptor weight ratio was 1:1.2, the weight ratio of 2-MN is 200% to the total mass of donor and acceptor, then an extra pre-annealing at 80 ^{o}C for 10 min was performed. The optimal active layer measured by a Bruker Dektak XT stylus profilometer was about 110 nm. A PNDIT-F3N layer via a solution concentration of 1 mg mL^{-1} was deposited at the top of the active layer at a rate of 4000 rpm for 30 s. Finally, the top argentum electrode of 100 nm thickness was thermally

evaporated through a mask onto the cathode buffer layer under a vacuum of ～5×10^{-6} mbar. The typical active area of the investigated devices was 4.8 mm^2. A non-refractive mask with a certified area of 2.89 mm^2 was used. The current-voltage characteristics of the solar cells were measured by a Keithley 2400 source meter unit under AM1.5G (100 mW cm^{-2}) irradiation from a solar simulator (Enlitech model SS-F5-3A). Solar simulator illumination intensity was determined at 100 mW cm^{-2} using a monocrystalline silicon reference cell with a KG5 filter. Short circuit currents under AM1.5G (100 mW cm^{-2}) conditions were estimated from the spectral response and convolution with the solar spectrum. The forward scan was adopted to test the *J-V* curves, and the scan step is 0.02 V and the delay time is 1 ms. The scan mode is sweep. The external quantum efficiency was measured by a Solar Cell Spectral Response Measurement System QE-R3011(Enli Technology Co., Ltd.).

Large-scale solar module fabrication: For the large-scale organic solar modules (5.0 cm × 5.0 cm. When fabricating the larger-area organic modules, the square ITO was patterned by laser ablation. After ITO-Cl was conducted, the active layer was coated through a doctor blade. After the PNDIT-F3N layer was deposited, the nanosecond laser (Coral GR12W-50K, Suzhou Microtreat Intelligent Technology Co., Ltd) with 532 nm pulse width was utilized to pattern the active layer (P2 line) for cell-to-cell connection and separate each sub-cell (P3 line) after the deposition of Ag. The femtosecond laser would not damage ITO at the bottom, and it would assist in forming good contact between sub-cells.

External quantum efficiency (EQE) measurements: The external quantum efficiency was measured by a Solar Cell Spectral Response Measurement System QE-R3011(Enli Technology Co., Ltd.).

Thermal stability testing: The testing devices were fabricated under the same preparation conditions as mentioned above. After the spin-coating of the active layer deposited on the ITO-Cl films, the samples were transferred to a hot plate at 120 °C in an N_2-filled glovebox and annealed for various periods. Then, the samples were quenched to room temperature before the cathode layers were thermally deposited. All the samples for time-dependent annealing measurements were prepared under the same conditions as the thermal stability testing.

Operational stability measurements: For the measurement of photostability, the devices were fabricated without further encapsulation. We performed light-induced degradation experiments with one sun equivalent illumination intensity for 1000 hours on these photovoltaic systems investigated in this study. The devices were put inside a nitrogen-filled glovebox (H_2O < 1 ppm, O_2 < 1 ppm) and continuously illuminated with a white LED array (XLamp CXA1512 6500K CCT). The illumination light intensity was initially set before testing to make sure the output short-circuit current density equals the value that was measured under standard conditions mentioned earlier, and it was monitored by a photodiode (Hamamtsu S1336-8BQ) to guarantee stable light intensity. *J-V* characteristics of the devices were checked periodically, and the photovoltaic parameters were calculated automatically according to the achieved *J-V* curves. Notably, the photovoltaic parameters of devices under illumination were recorded over time, and the degradation curves were shown. The cell temperature was measured occasionally, and the temperature range during aging was approximately 30 ℃.

Experimental details of transient absorption spectroscopy (TAS): Femtosecond transient absorption spectroscopy measurements were performed on an Ultrafast Helios pump-probe system in collaboration with a regenerative amplified laser system from Coherent. An 800 nm pulse with a repetition rate of 1kHz, a length of 100 fs, and an energy of 7 mJ/pluse was generated by a Ti: sapphire amplifier (Astrella, Coherent). Then the 800 nm pulse was separated into two parts by a beam splitter. One part was coupled into an optical parametric amplifier (TOPAS, Coherent) to generate the pump pulses at 800 nm. The other part was focused on a YAG plate to generate a white light supercontinuum as the probe beams with spectra covering 750-1600 nm. The time delay between pump and probe was controlled by a motorized optical delay line with a maximum delay time of 8 ns. The sample films were spin-coated onto the 1 mm-thick quartz plates and are encapsulated by epoxy resin in a nitrogen-filled glove box to resist water and oxygen in the air. The pump pulse is chopped by a mechanical chopper at 500 Hz and then focused onto the mounted sample with probe beams. The probe beam was collimated and focused into a fiber-coupled multichannel spectrometer with a CCD sensor. The energy of the pump pulse was measured and calibrated by a power meter (PM400, Thorlabs).

Temperature-dependent PL spectra measurements: Temperature-dependent PL spectra were collected using a HORIBA iHR320 spectrometer. The sample temperature was varied from 78 K to 298 K in steps of 20 K. A continuous-wave 405 nm laser was used as the excitation source. All measurements were performed on thin-film samples deposited on glass substrates. The temperature dependence of the integrated photoluminescence (PL) intensity for the PYT, D-SeV-Cl, and PYT:D-SeV-Cl blend films was analyzed using the Arrhenius quenching model. This model is widely employed to describe the thermal deactivation of excitons or charge carriers via non-radiative recombination channels in semiconductors. The integrated PL intensity I(T) as a function of absolute temperature T is described by:

$$I(T) = \frac{I_0}{1 + A\ exp(-\frac{E_b}{k_B T})}$$

where: I(T) is the integrated PL intensity at temperature T; I_0 is the PL intensity extrapolated to the low-temperature limit; A is a dimensionless pre-exponential factor related to the ratio of non-radiative to radiative recombination rates; E_b is the exciton binding energy; k_B is the Boltzmann constant.

Transient photocurrent (TPC) measurements: Relevant control and MSM solar cells were excited with a 405 nm laser diode. The transient photocurrent response of the devices at a short circuit condition to a 200 μs square pulse from the LED with no background illumination. The current traces were recorded on a Tektronix DPO3034 digital oscilloscope by measuring the voltage drop over a 5-ohm sensor resistor in series with the solar cell. A DC voltage was applied to the solar cell with an MRF544 bipolar junction transistor in a common collector amplifier configuration.

Transient photovoltage (TPV) measurements: In the TPV measurements, a 405 nm laser diode was used to keep the organic solar cells in the V_{oc} conditions. Measuring the light intensity with a highly linear photodiode and driving the laser intensity with a waveform generator (Agilent 33500B) at one sun. Moreover, a small perturbation was induced with a second 405 nm laser diode. The intensity of the short laser pulse was adjusted to keep the

voltage perturbation below 10 mV. After the pulse, the voltage decays back to its steady state value in a single exponential decay.

Photo-induced charge carrier extraction by linearly increasing the voltage (photo-CELIV) measurements: In photo-CELIV measurements, the devices were illuminated with a 405 nm laser diode. Current transients were recorded across the internal 50 Ω resistor of our oscilloscope. Here, a fast electrical switch was used to isolate the device to prevent carrier extraction or sweep-out. After the variable delay time, the switch connected the device to a function generator. It applied a linear extraction ramp, which was 40 μs long and 2.0 V high. Moreover, it started with an offset matching the V_{OC} of the device for each delay time. To determine the mobility in the devices, photo-CELIV curves were measured using different experimental conditions, differing in delay time and applied voltage.

Molecular dynamics simulation: To investigate the assembly behavior in PYT/D-SeV-Cl (1.2:0.05 wt/wt) systems, we conducted all-atom molecular dynamics (AA-MD) simulations using the GROMACS 2021 software suite, equipped with the General Amber Force Field (GAFF).[2, 3] The atom charges were fitted using the Restrained Electrostatic Potential (RESP) method, employing the B3LYP functional and the 6-31 basis set. Two additional systems comprising pure PYT and D-SeV-Cl were established as controls. By employing a generalized film formation method, we closely mirrored the experimental conditions to reproduce the molecular self-assembly behavior in thin films. During the simulations, the LINCS algorithm was utilized to constrain the covalent bonds involving H atoms.[4] The simulation time step was set to 1.0 fs, and all simulations were conducted under periodic boundary conditions. Pressure and temperature were controlled using the Parrinello–Rahman barostat set to 1 atm and the V-rescale thermostat, respectively.[5, 6] The nonbonded interactions were truncated at a cut-off distance of 12 Å, while the particle mesh Ewald (PME) method was employed to compute long-range electrostatic interactions.[7] Finally, graphics and visualization analyses were handled by the Visual Molecular Dynamics (VMD) program.[8]

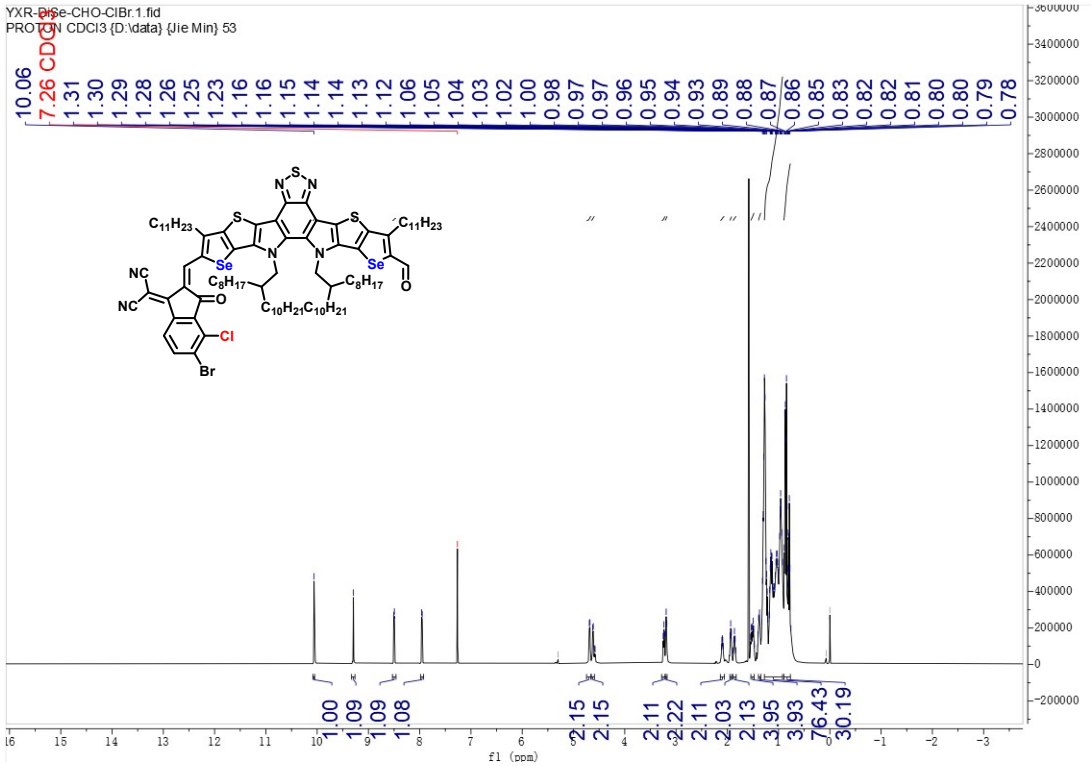

Figure S1. ^{1}H NMR of compound II.

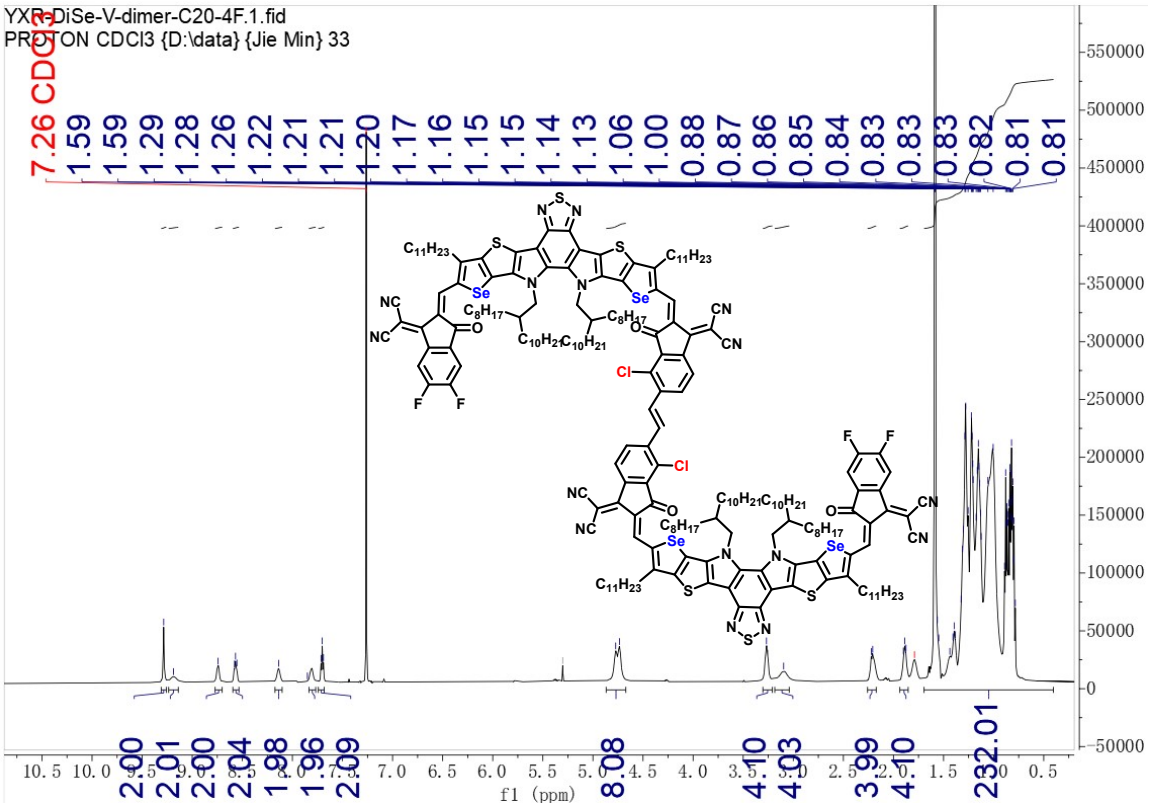

Figure S2. ^{1}H-NMR spectrum of D-SeV-Cl.

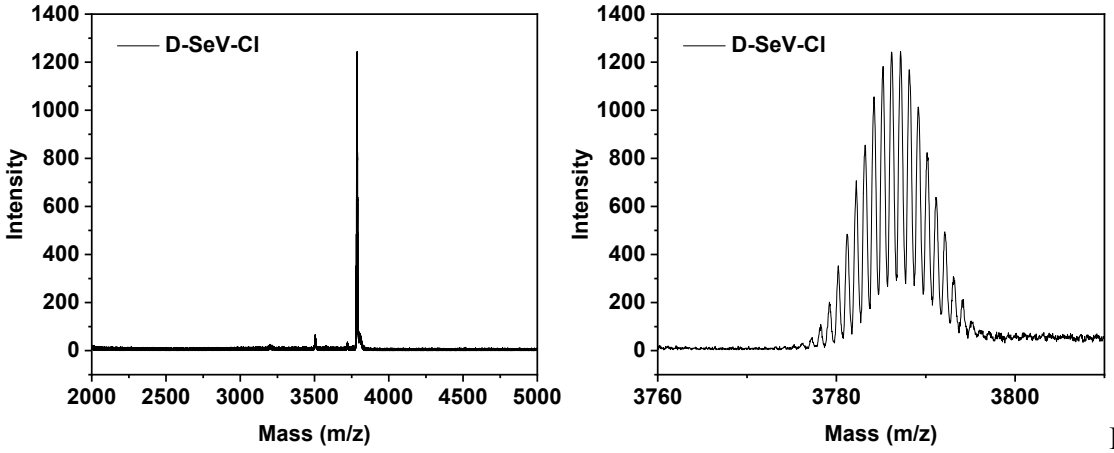

Figure S3. Mass spectrum of D-SeV-Cl.

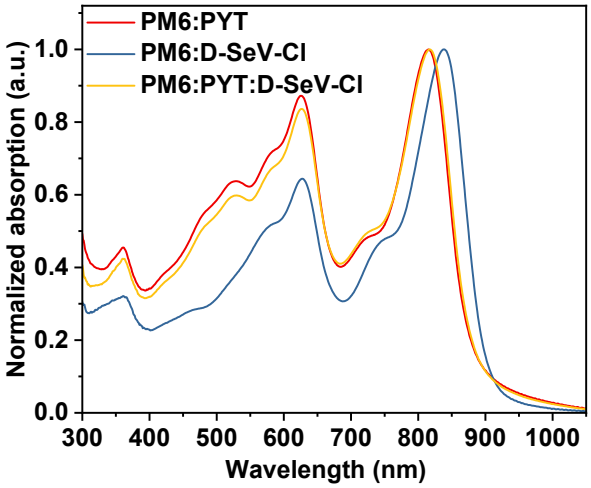

Figure S4. The normalized absorption spectra of PM6:PYT, PM6:D-SeV-Cl and PM6:PYT:D-SeV-Cl (1:1.2:0.05, wt%) in thin films.

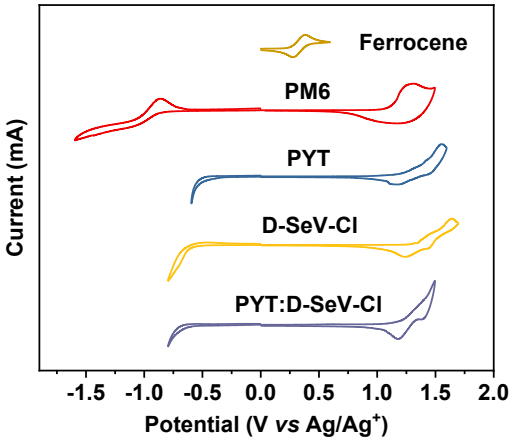

Figure S5. Cyclic voltammetry curves of Ferrocene, PM6, PYT, D-SeV-Cl and PYT:D-SeV-Cl in acetonitrile solution with 0.1 M n-Bu_4PF_6 as the supporting electrolyte, at a scanning rate of 100 mV s^{-1}.

Table S1. Optical and electrochemical properties of the tested materials.

Materials	$\lambda_{max,\ film}$ (nm)	$\lambda_{onset,\ film}$ (nm)	E_g[a] (eV)	LUMO/HOMO[b] (eV)
PM6	616	686	1.807	-3.61/-5.58
PYT	804	874	1.421	-3.88/-5.73
D-SeV-Cl	854	923	1.343	-3.96/-5.80
PYT:D-SeV-Cl	/	/	/	-3.91/-5.71

[a)]Calculated from the absorption onset of the films. [b)]Estimated from the reduction/oxidation onset of the CV curves.

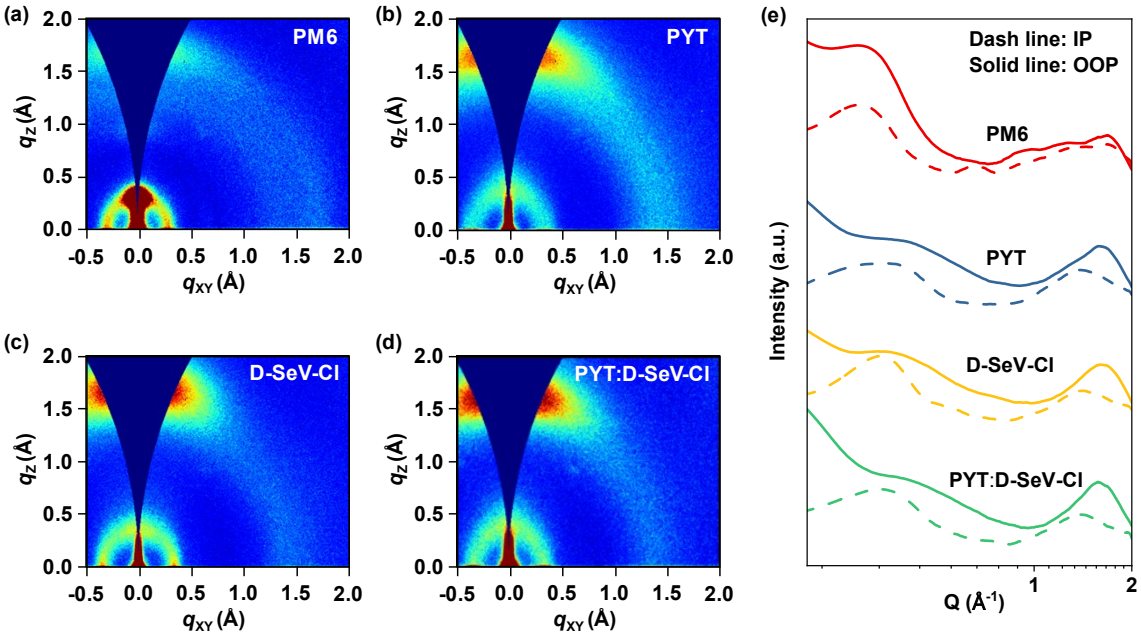

Figure S6. 2D GIWAXS patterns of pristine (a) PM6, (b) PYT, (c) D-SeV-Cl (d) blend PYT:D-SeV-Cl. (e) IP and OOP extracted line-cut profiles of relevant films. All polymer donor and acceptor films exhibited well-defined crystalline structures with a predominant face-on orientation concerning the substrate. PM6 films displayed a weak (010) π-π stacking peak (q_z = 1.707 Å^{-1}) and a (100) lamellar peak (q_z = 0.298 Å^{-1}) in the out-of-plane (OOP) direction.

Table S2. Investigations of the morphology parameters extracted from the GIWAXS measurements of the PM6, PYT, D-SeV-Cl and PYT:D-SeV-Cl films.

Neat films	In plane (100)		Out of plane (010)			
	Q (Å^{-1})	d (Å)	Q (Å^{-1})	d (Å)	FWHM (Å^{-1})	CCL (Å)
PM6	0.298	21.07	1.707	3.67	0.542	11.58
PYT	0.351	17.89	1.581	3.97	0.315	19.93
D-SeV-Cl	0.337	18.63	1.612	3.89	0.280	22.42
PYT:D-SeV-Cl	0.340	18.47	1.577	3.98	0.268	23.43

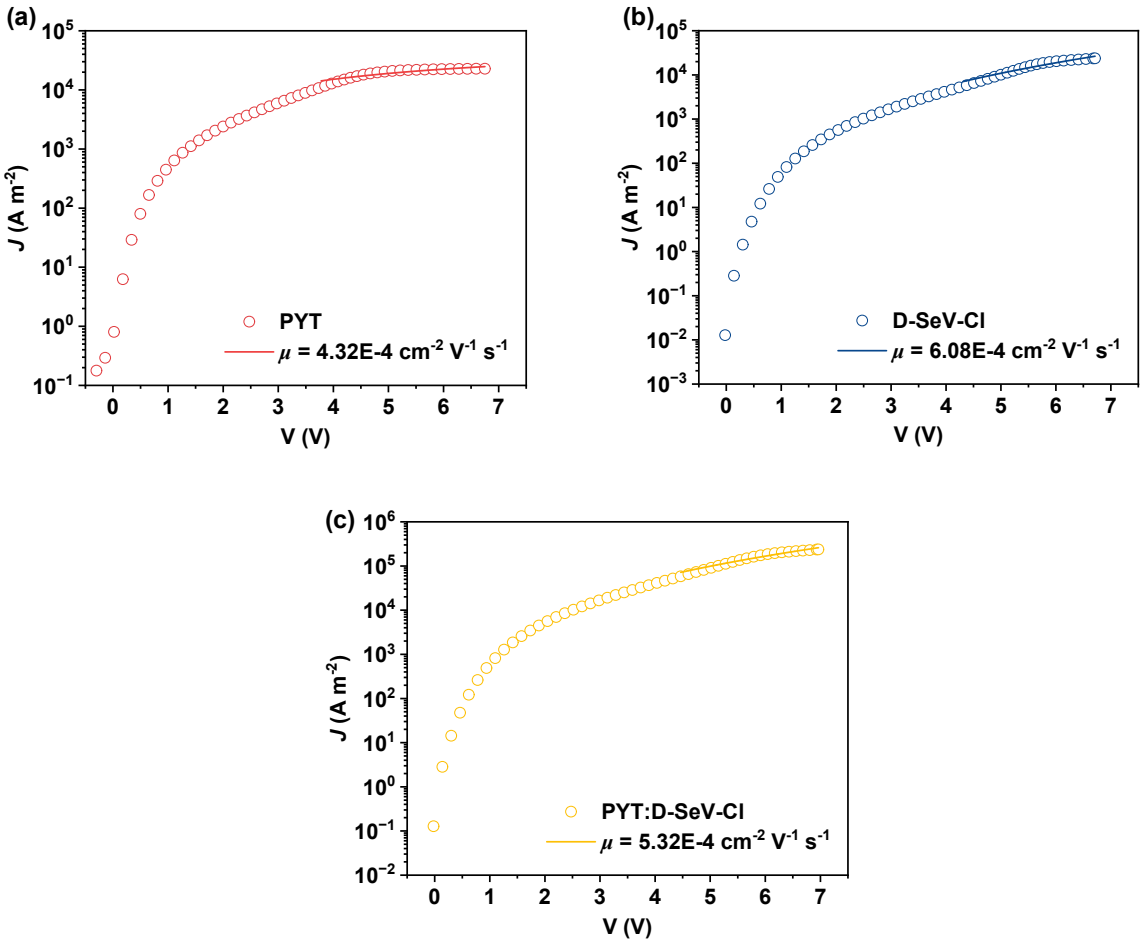

Figure S7. The dark *J-V* characteristics of pristine (a) PYT, (b) D-SeV-Cl and (c) PYT: D-SeV-Cl-based electron-only devices. The solid lines represent the best fit using the SCLC model.

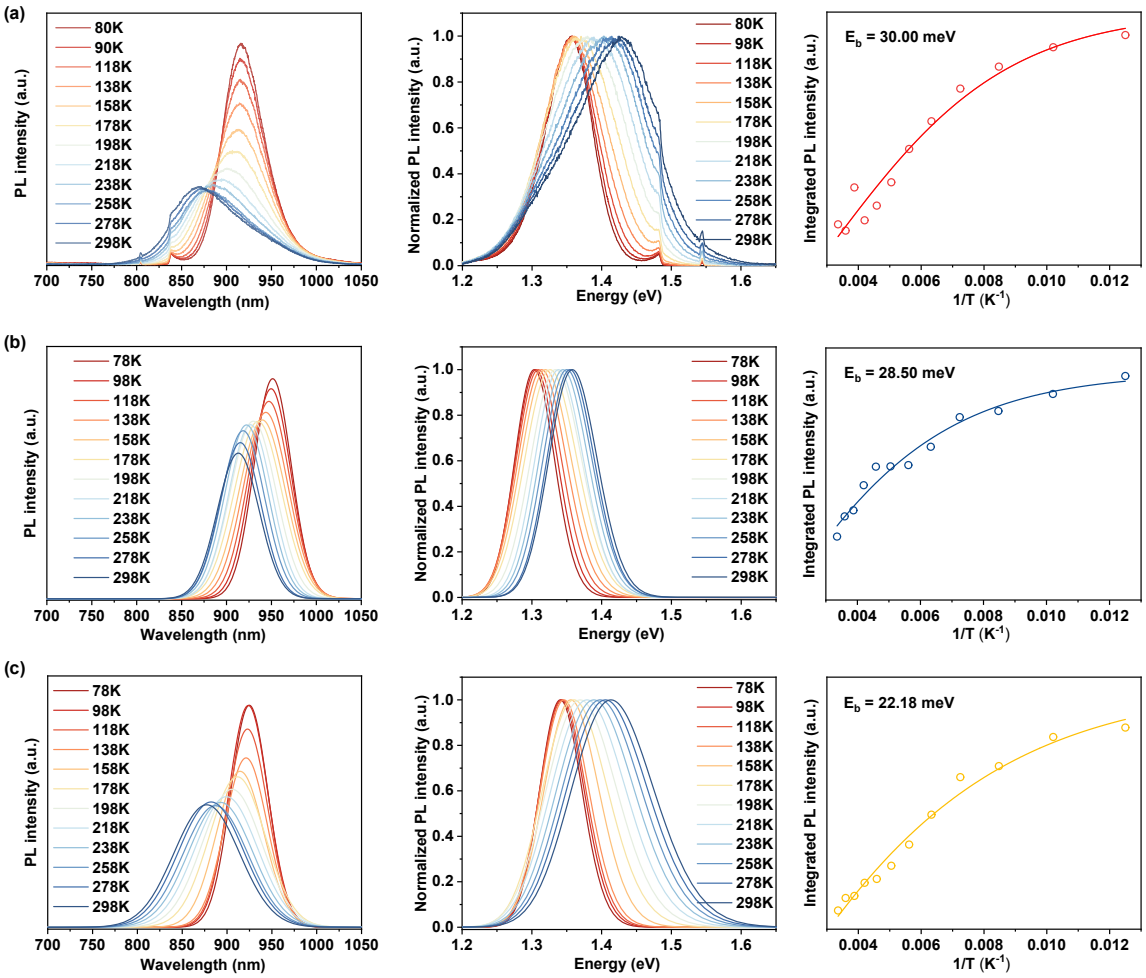

Figure S8. The temperature-dependent PL spectra for the (a) PYT, (b) D-SeV-Cl and (c) PYT:D-SeV-Cl films.

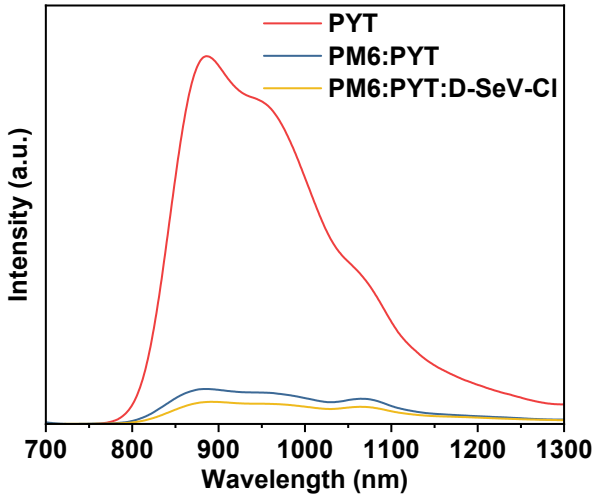

Figure S9. The PL spectra of the neat PYT film and the PM6:PYT blend films treated without and with D-SeV-Cl dimer.

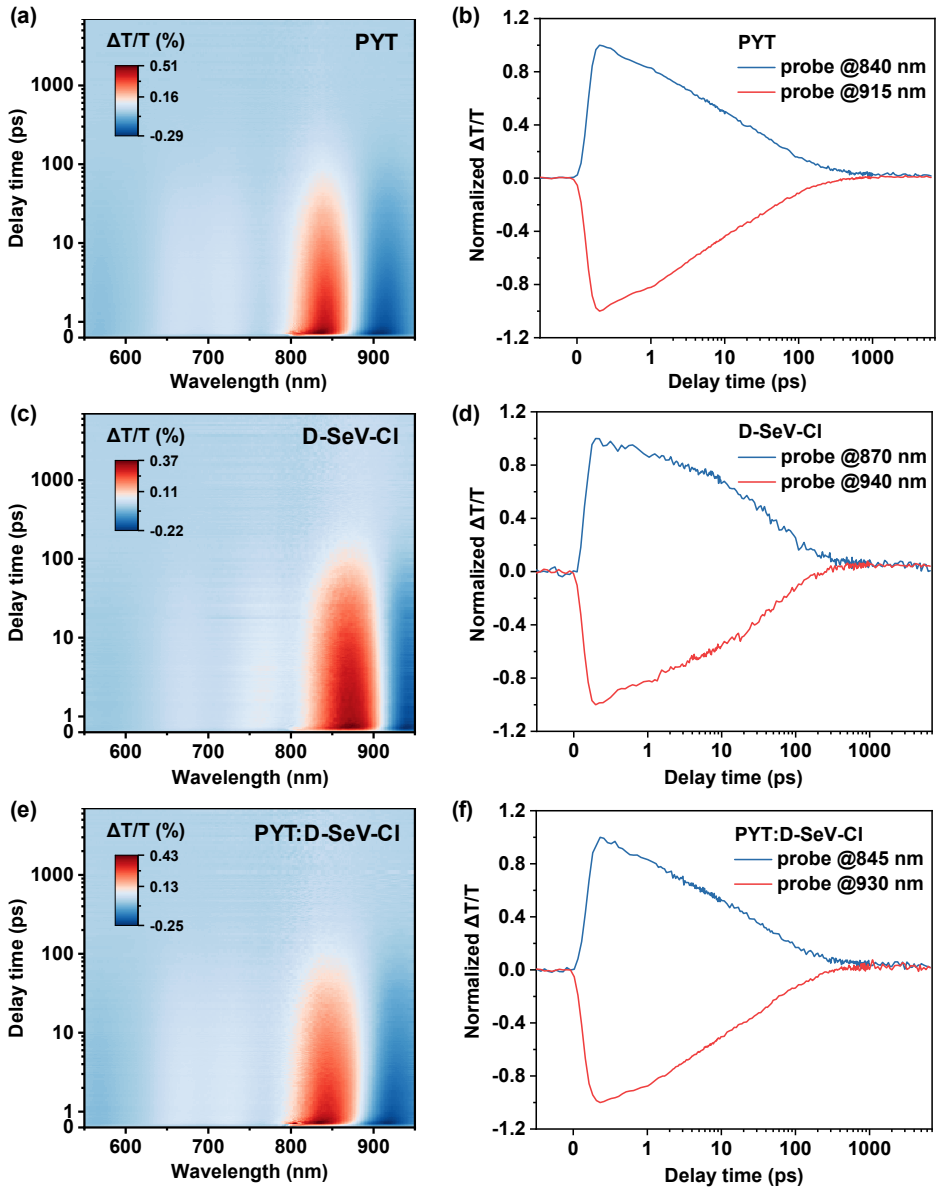

Figure S10. The TA images of (a) PYT, (b) D-SeV-Cl neat film and (c) PYT:D-SeV-Cl blend film.

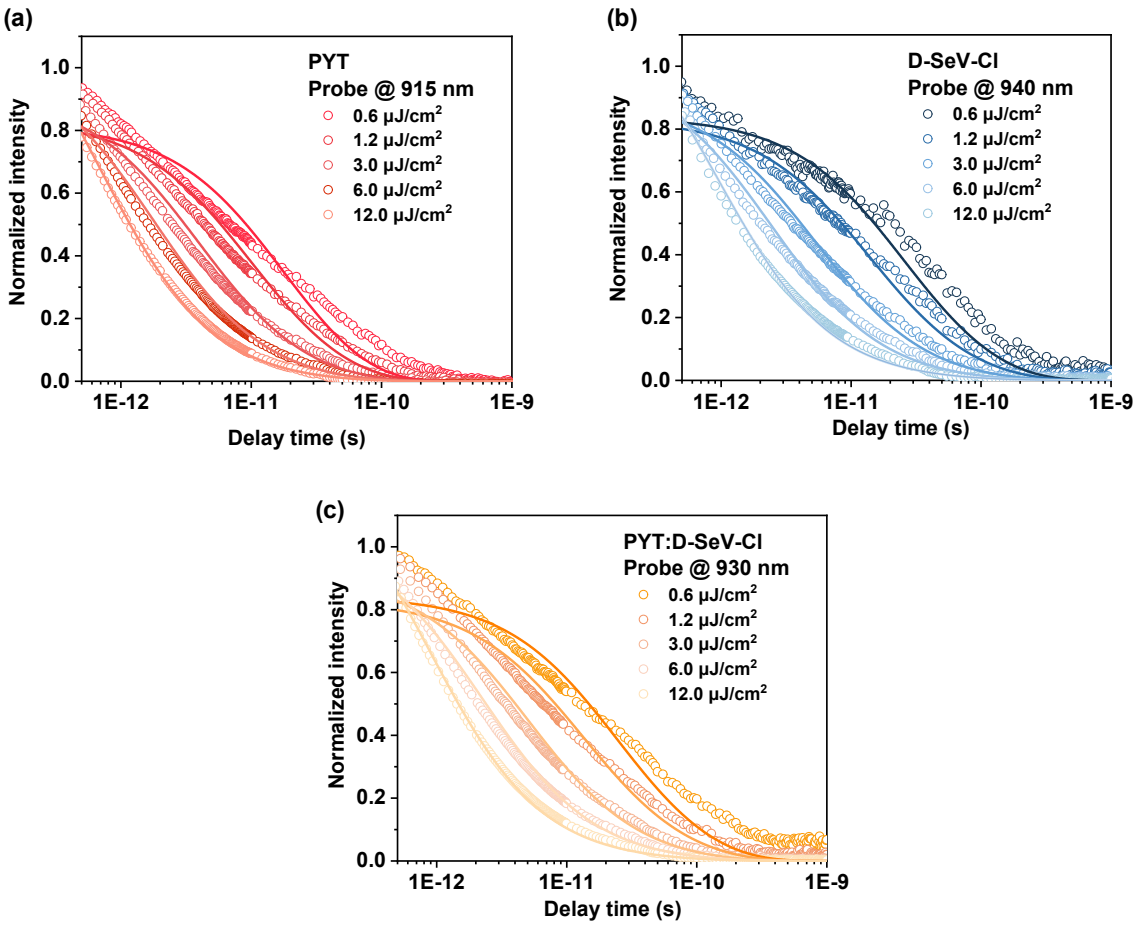

Figure S11. The decay dynamics of the singlet excitons in (a) PYT, (b) D-SeV-Cl neat film and (c) PYT:D-SeV-Cl blend film under 800 nm pump with power fluxes of 0.6, 1.2, 3.0, 6.0 and 12.0 μJ cm^{-2}.

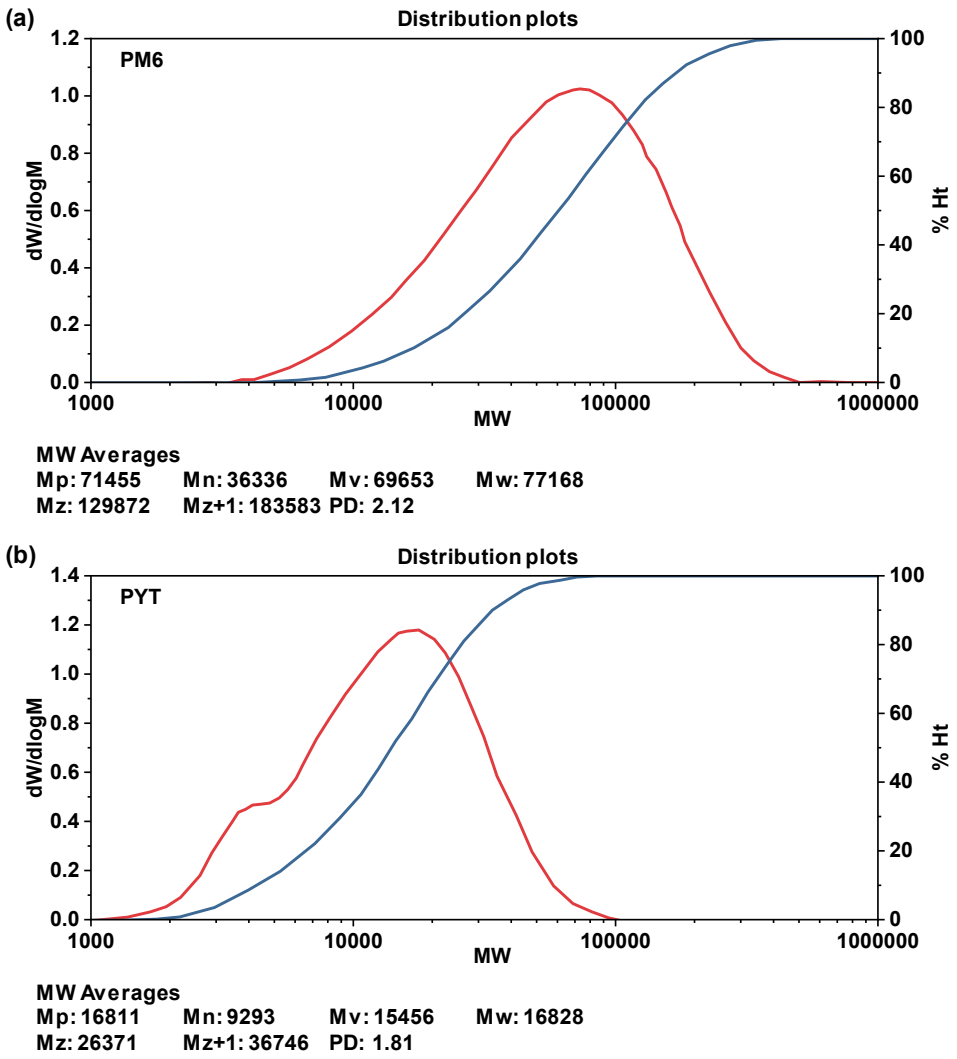

Figure S12. Molecular weight values of polymer donor PM6 and polymer acceptors PYT obtained by GPC with 1,2,4-trichlorobenzene as the eluent at 150 °C.

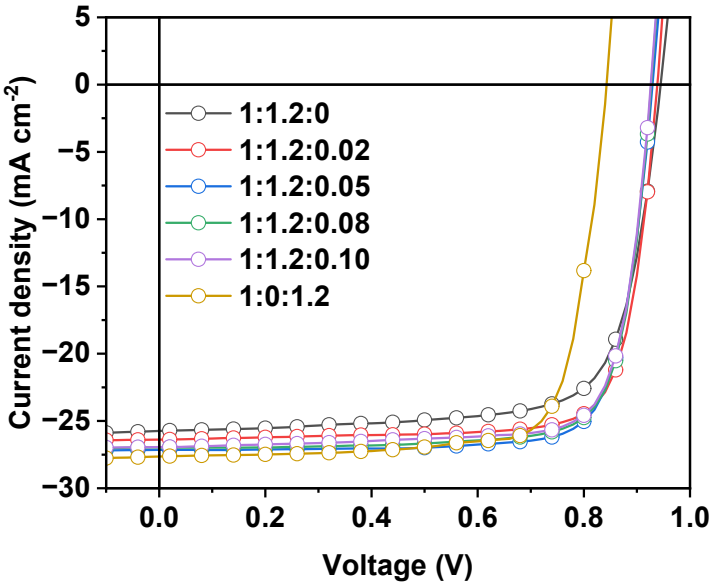

Figure S13. *J-V* curves of the organic solar cells with different D-SeV-Cl contents measured under the illumination of AM 1.5G at 100 mW cm^{-2}.

Table S3. Photovoltaic parameters of the organic solar cells with different D-SeV-Cl contents, measured under the illumination of AM 1.5G at 100 mW cm^{-2}.

PM6:PYT:D-SeV-Cl	V_{OC} [V]	J_{SC} [mA cm^{-2}]	FF [%]	PCE[a] [%]
1:1.2:0	0.944 (0.940±0.005)	25.75 (25.42±0.1)	74.29 (73.00±0.2)	18.06 (17.84±0.2)
1:1.2:0.02	0.938 (0.880±0.004)	26.39 (26.20±0.2)	78.78 (78.50±0.3)	19.50 (19.35±0.1)
1:1.2:0.05	0.932 (0.928±0.005)	27.15 (26.88±0.1)	79.11 (78.95±0.1)	20.01 (19.70±0.2)
1:1.2:0.08	0.927 (0.925±0.005)	26.97 (26.80±0.2)	79.20 (78.75±0.2)	19.80 (19.65±0.2)
1:1.2:0.10	0.926 (0.924±0.005)	26.94 (26.80±0.2)	78.82 (78.30±0.1)	19.66 (18.45±0.1)
1:0:1.2	0.843 (0.838±0.006)	27.64 (27.40±0.1)	77.32 (76.50±0.1)	18.01 (17.90±0.1)

[a]The values in parentheses are the average PCEs obtained from 10 devices.

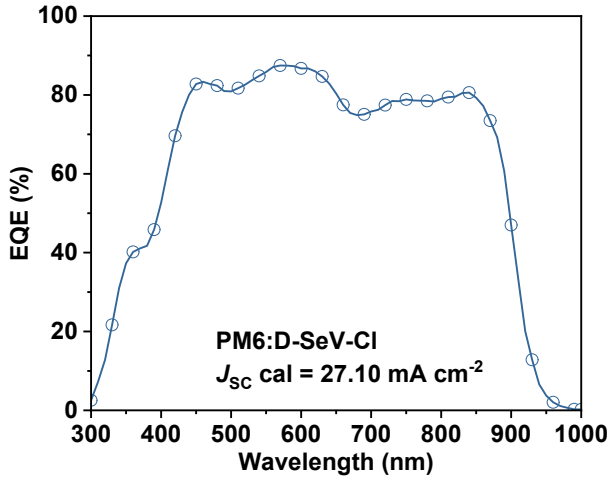

Figure S14. EQE curve and J_{SC} values calculated from EQE curve of the PM6:D-SeV-Cl based device.

Table S4. Data points gathered from published studies on all-polymer solar cells processed by linear-coating technology. The publication years, photovoltaic parameters, champion PCEs and materials used are summarized below. The corresponding references can be found at the end of the supporting information.

Year	V_{OC} (V)	J_{SC} (mA cm^{-2})	FF (%)	PCE (%)	Systems	Reference
2017	0.64	15.5	50	5.10	PTB7-Th:PPDIE	[9]
2019	0.88	17.62	75.58	11.76	PTzBI-Si:N2200	[10]
2021	0.787	11.2	51	4.50	PTB7-Th:P(NDI2OD-2T)	[11]
2021	0.891	23.03	73.98	15.17	PBDB-T:PYT	[12]
2021	1.25	8.31	53.8	5.59	CD1:PBN-21	[13]
2021	0.901	22.6	63.4	13.0	PM6:PYF-T-o	[14]
2022	0.874	19.4	53.9	9.14	PBDB-T:PYSe	[15]
2022	0.894	21.3	62.2	11.84	PBDB-T:PYSe-TCl20	[15]
2022	0.908	22.3	68.1	12.83	PBDB-T:PYSe-TCl20:PTClo-Y	[15]
2022	0.948	19.99	65.7	12.42	Y5-Br:PTClo-Y	[16]
2022	0.89	23.05	65.52	13.44	PM6:PBN26	[17]
2022	0.891	22.94	66.26	13.54	PBDB-T:PYSe-TC6T (10)	[18]
2022	0.945	23.27	70.77	15.53	PM6:PY-IT	[19]
2022	0.94	13.09	52.1	6.43	PBDBT:PF5-Y5	[20]
2023	0.92	15.7	60	8.66	PBDBT:PF5-Y5	[21]
2025	0.922	25.66	77.19	18.26	PM6:PY-TYTz-5	[22]
2025	0.930	26.60	78.65	19.46	(D18-Cl:PY-Cl)/(PM6:PY-SSe)	[23]
2025	0.932	27.15	79.11	20.01	PM6:PYT:D-SeV-Cl	This work

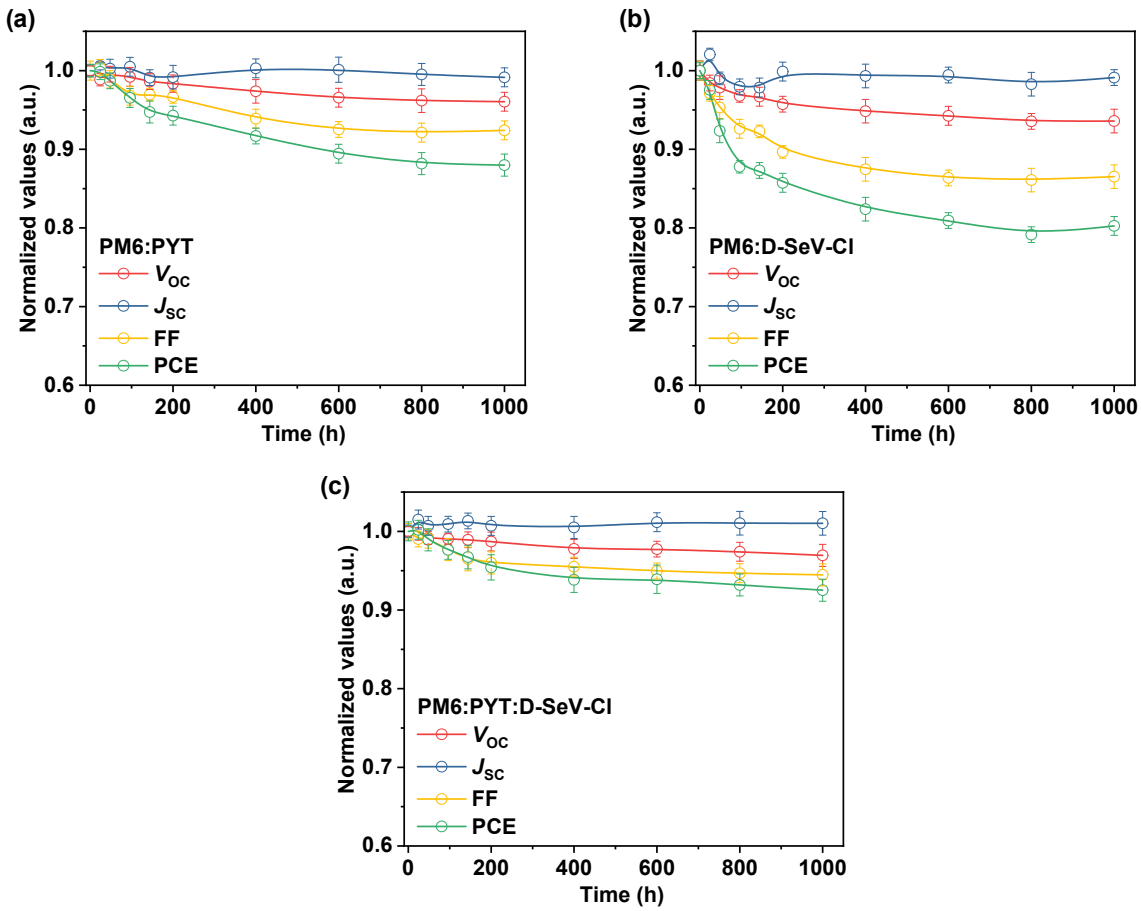

Figure S15. The normalized degradation trends of relevant photovoltaic parameters of the (a) PM6:PYT, (b) PM6:D-SeV-Cl and (c) PM6:PYT:D-SeV-Cl systems, including PCE, FF, J_{SC} and V_{OC}, under continuous thermal annealing at 120 °C.

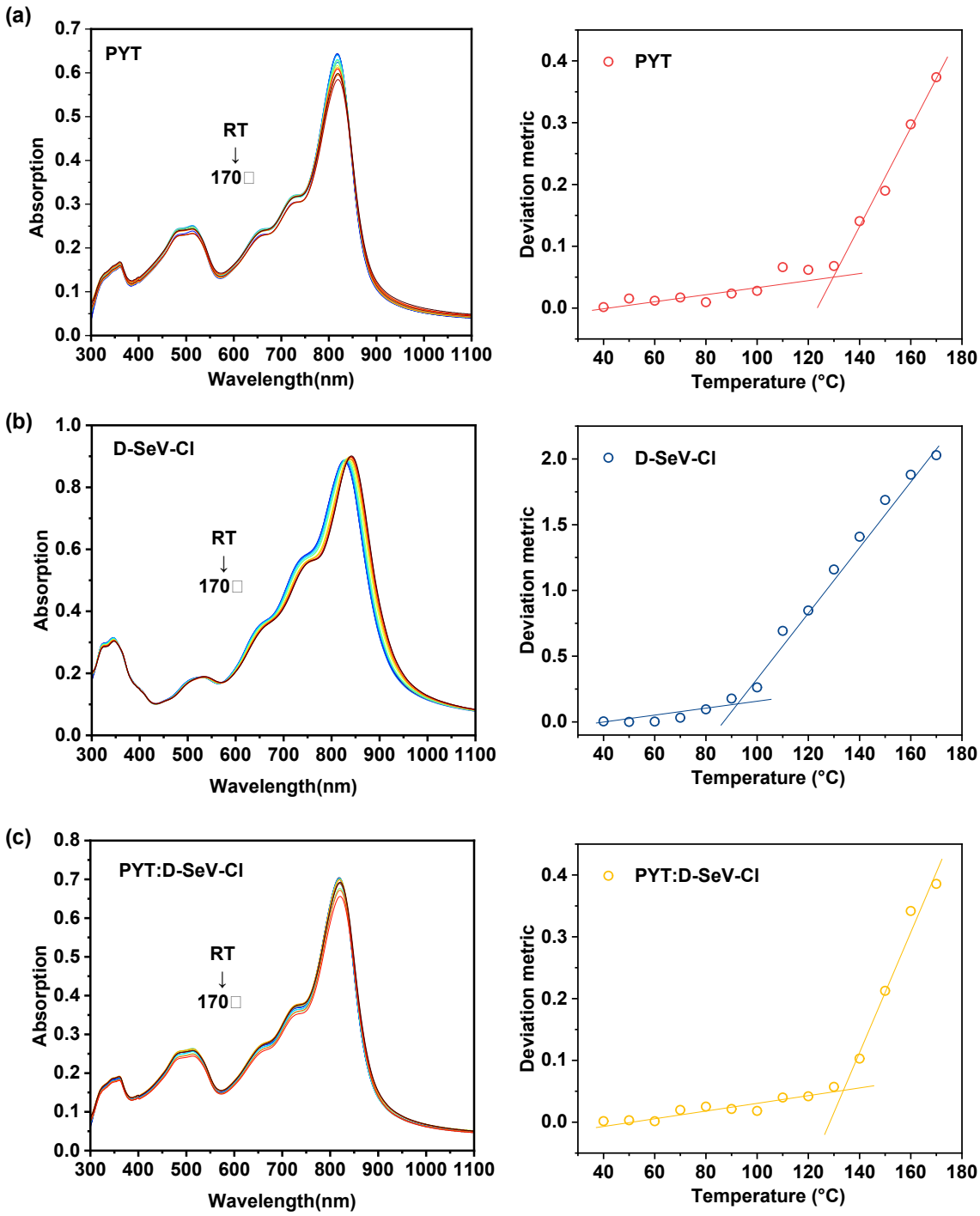

Figure S16. *UV–vis-NIR* absorption spectra and deviation metric of redshifts with the increasing thermal annealing temperature of (a) PYT, (b) D-SeV-Cl and (c) PYT:D-SeV-Cl films.

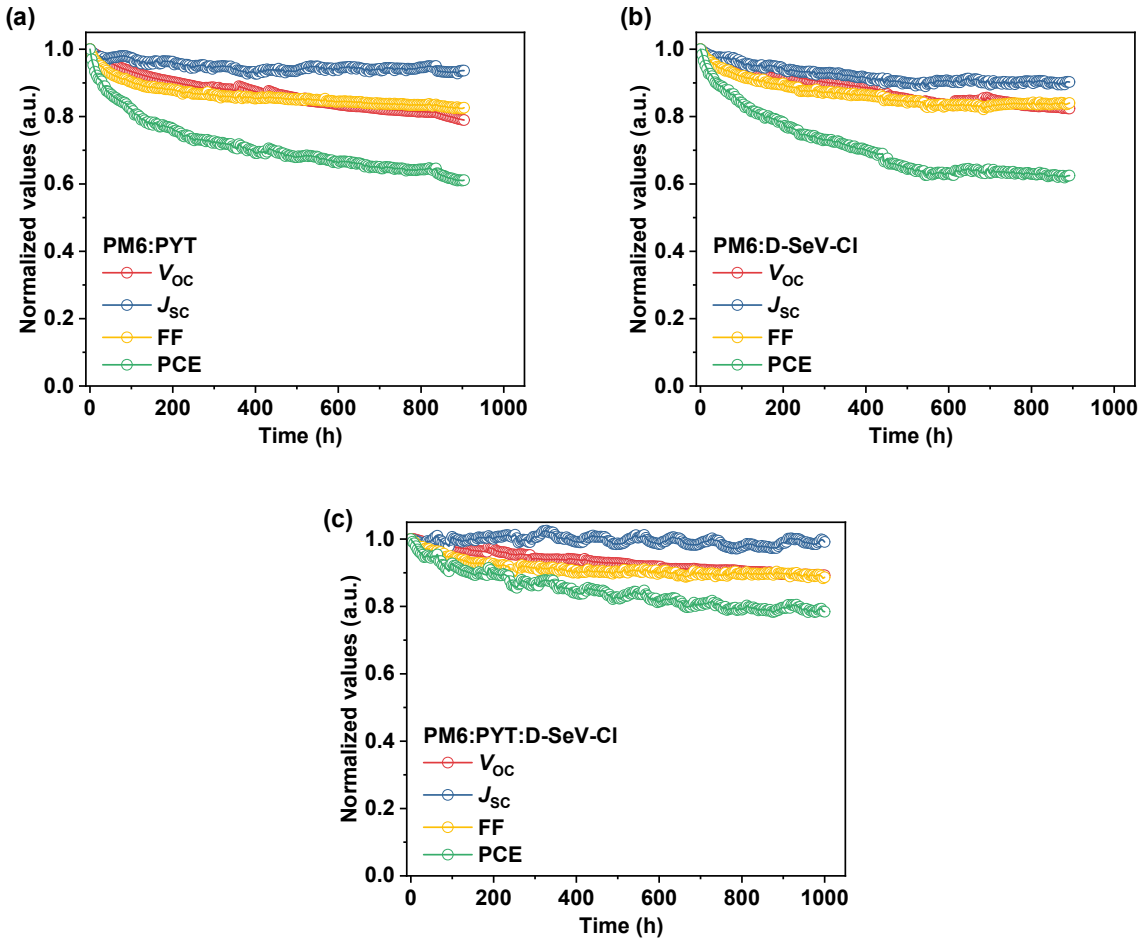

Figure S17. The normalized degradation trends of relevant photovoltaic parameters of the (a) PM6:PYT, (b) PM6:D-SeV-Cl and (c) PM6:PYT:D-SeV-Cl systems, including PCE, FF, J_{SC} and V_{OC}, with maximum power point tracking under the continuous light-emitting diode (LED) lighting condition for about 1000 hours.

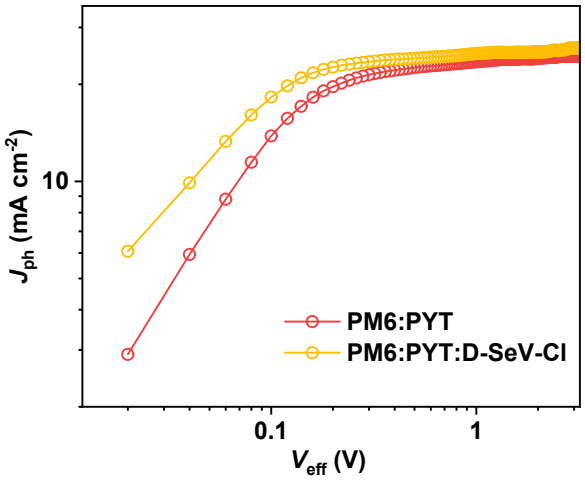

Figure S18. The J_{ph}-V_{eff} curves of PM6:PYT and PM6:PYT:D-SeV-Cl (1:1.2:0.05, wt%)-based devices.

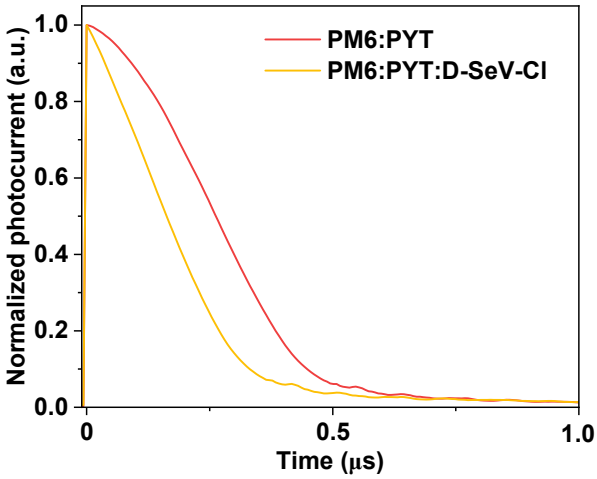

Figure S19. The normalized TPC data for the PM6:PYT and PM6:PYT:D-SeV-Cl devices.

Table S5. The parameters of exciton dissociation efficiency and charge collection efficiency.

Active layer	η_{diss}[a)] [%]	S[b)]	α[c)]	τ_{TPC}[d)] [μs]	R[e)]	ε_r[f)]
PM6:PYT	96.23	0.995	1.52	0.38	2.78	3.00
PM6:PYT:D-SeV-Cl	97.92	0.998	1.42	0.24	2.36	3.76

a)Under short circuit condition.

b)$J_{sc} \propto P_{in}^{\alpha}$.

c)$V_{oc} \propto (nkT/q)\ln P_{in}$.

d)The extraction time extract from TPC.

e)The non-geminate recombination order R was determined via combining TPV and CE measurements.

f)Dielectric constant.

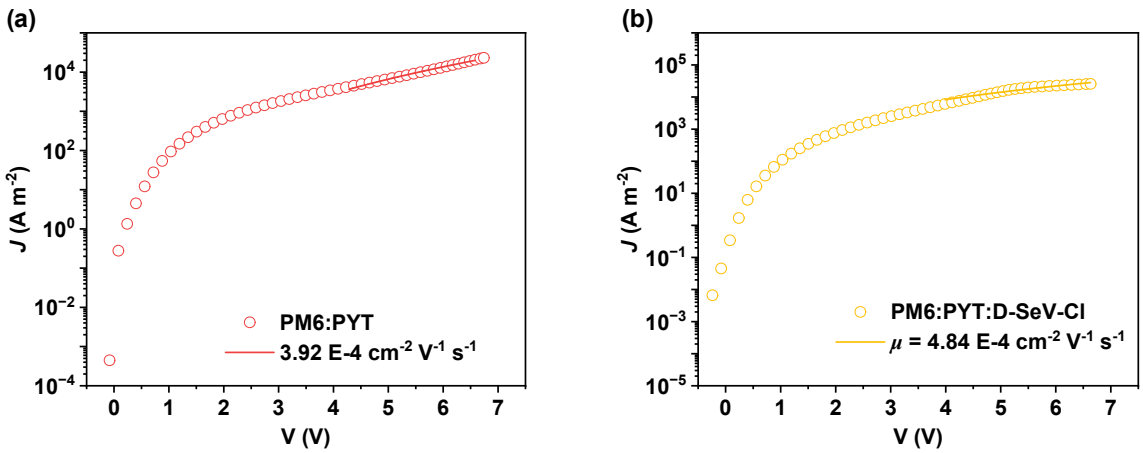

Figure S20. The dark *J*-*V* characteristics of PM6:PYT all-polymer systems treated (a) without and (b) with D-SeV-Cl dimer additive based hole-only devices. The solid lines represent the best fit using the SCLC model.

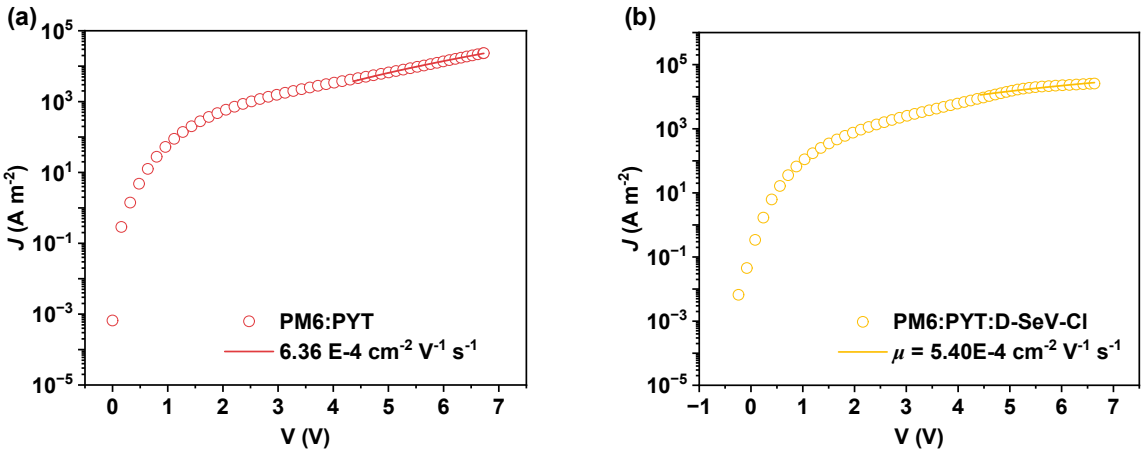

Figure S21. The dark *J-V* characteristics of PM6:PYT all-polymer systems treated (a) without and (b) with D-SeV-Cl dimer additive based electron-only devices. The solid lines represent the best fit using the SCLC model.

Table S6. Hole and electron mobilities of the blended films were determined from the SCLC measurements.

Active layer	Hole-only [$\times 10^{-4}$ $cm^2V^{-1}s^{-1}$]	Electron-only [$\times 10^{-4}$ $cm^2V^{-1}s^{-1}$]	Electron-only/ Hole-only
PM6:PYT	3.92±0.26	6.36±0.22	1.62
PM6:PYT:D-SeV-Cl	4.89±0.25	5.40±0.24	0.91

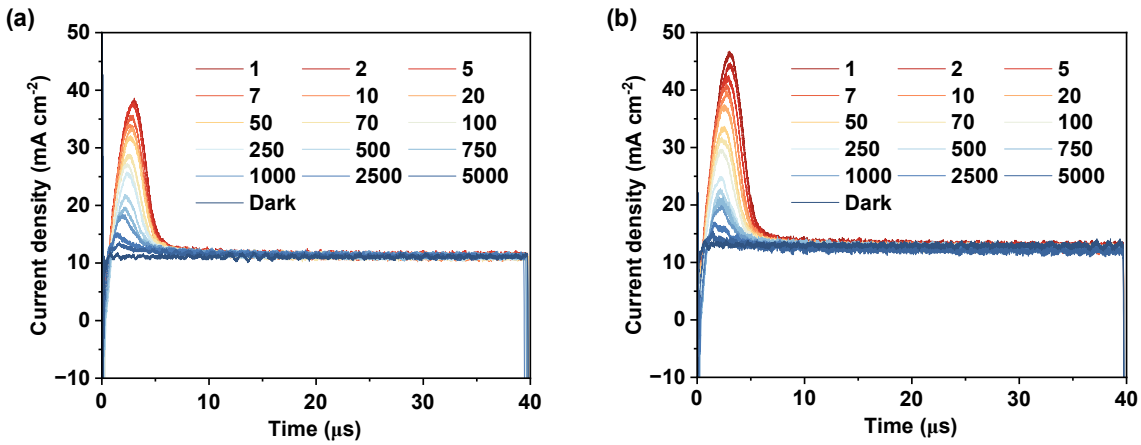

Figure S22. The Photo-CELIV traces of PM6:PYT all-polymer systems treated (a) without and (b) with D-SeV-Cl dimer additive based devices for different delay times between the light pulse and the extraction voltage ramp.

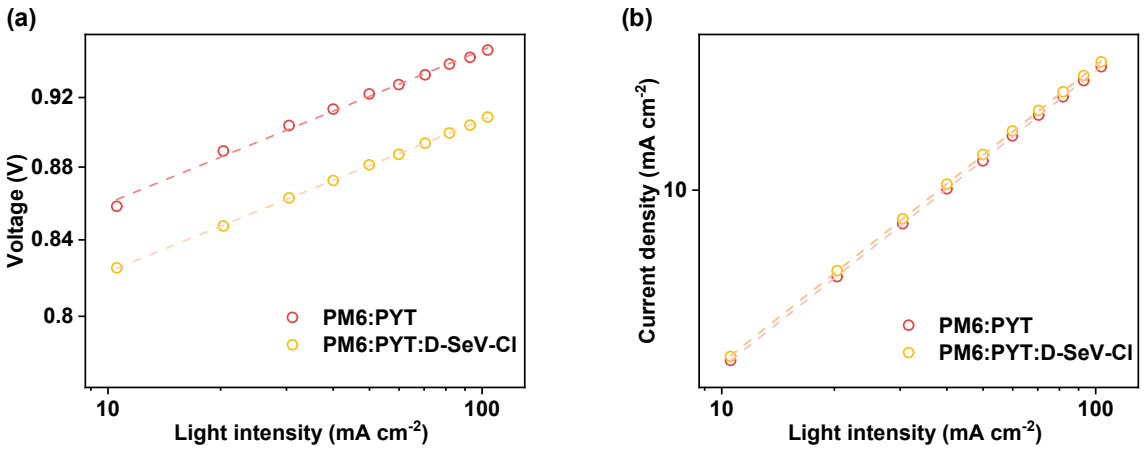

Figure S23. The (a) V_{OC} and J_{SC} versus light intensity characteristics of PM6:PYT all-polymer systems treated (a) without and (b) with D-SeV-Cl dimer additive-based devices.

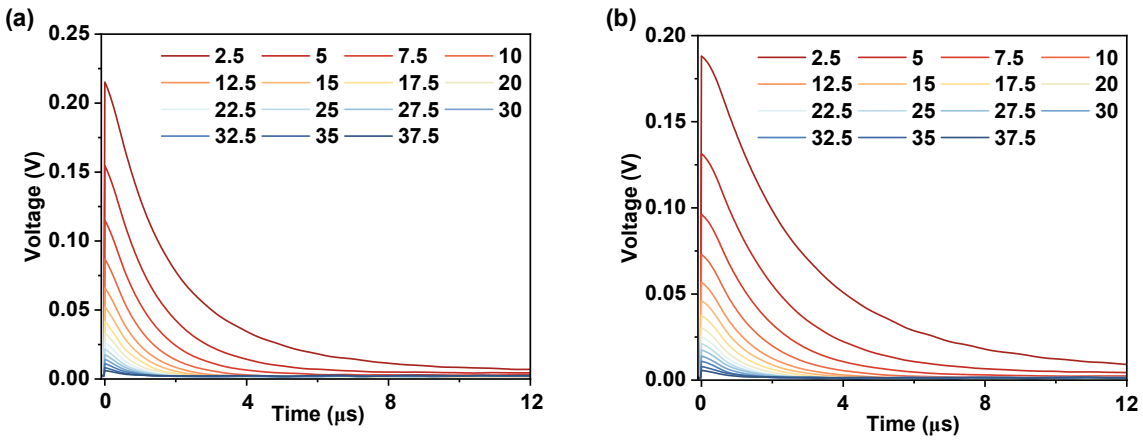

Figure S24. The TPV measurements on the optimized PM6:PYT all-polymer systems treated (a) without and (b) with D-SeV-Cl dimer additive-based devices.

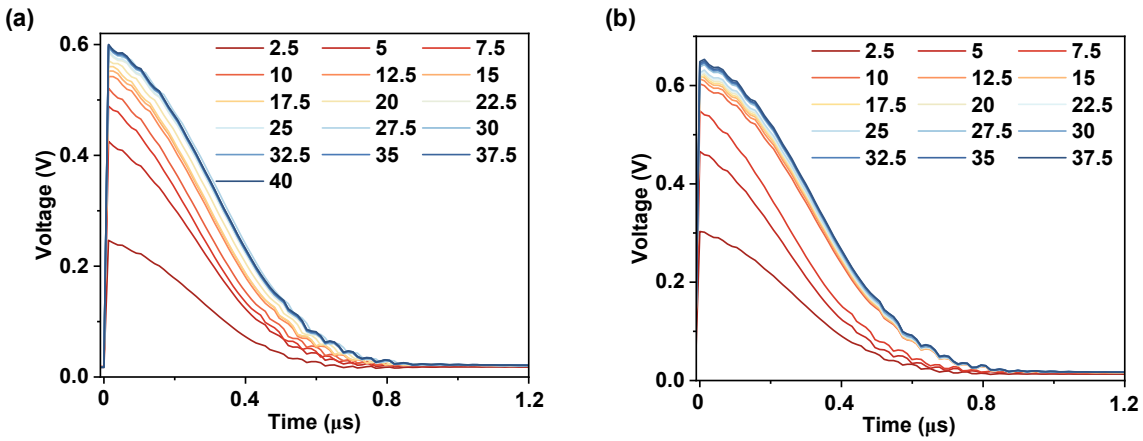

Figure S25. The CE measurements on the optimized PM6:PYT all-polymer systems treated (a) without and (b) with D-SeV-Cl dimer additive-based devices.

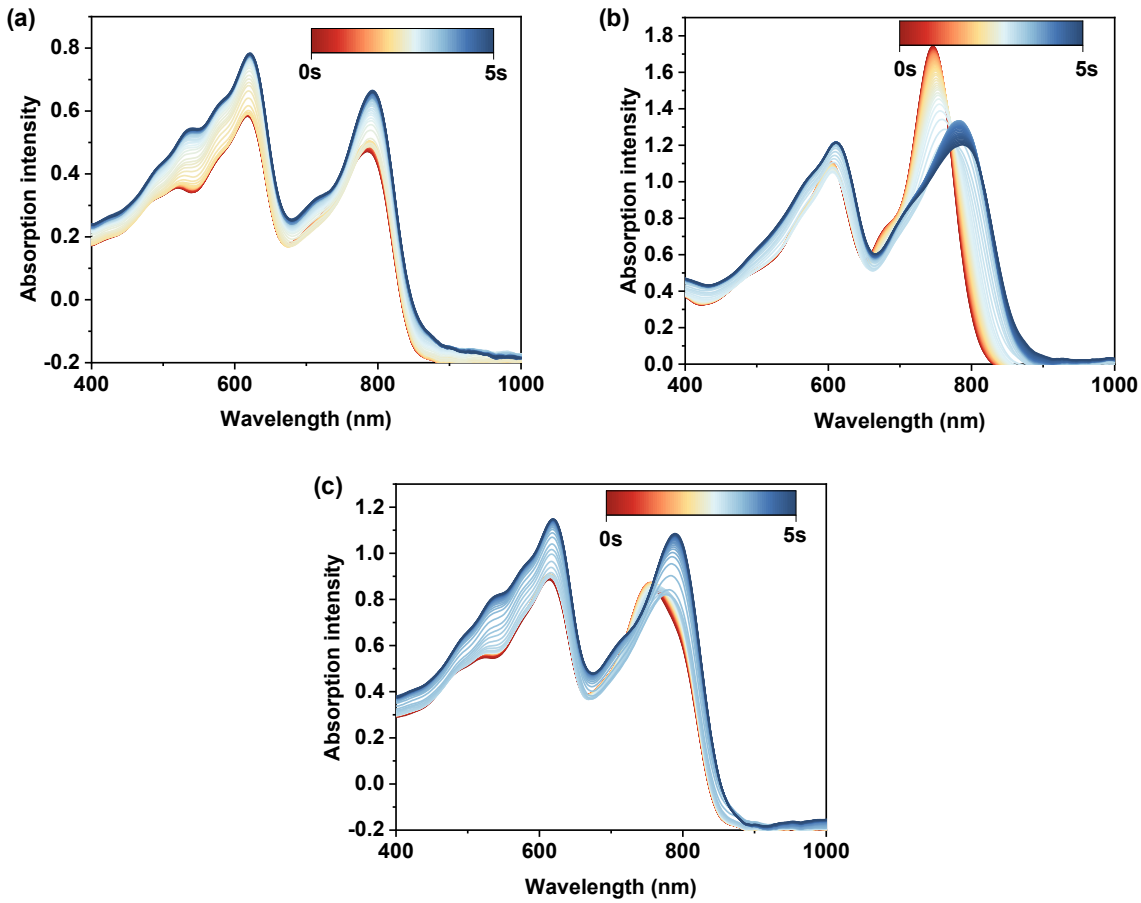

Figure S26. Evolution of in-situ UV during the film formation processes of the (a) PM6:PYT, (b) PM6:D-SeV-Cl and (c) PM6:PYT:D-SeV-Cl active layers fabricated at the same coating speed.

Table S7. Comparative analysis of packing distance (unit: Å) and packing number in pristine PYT, D-SeV-Cl, and PYT:D-SeV-Cl blend systems.

Films	Core-Core	Core-Terminal	Terminal-Terminal	Total
PYT	4.09/111	4.07/337	4.04/243	4.06/691
D-SeV-Cl	4.12/88	4.04/223	3.90/189	4.00/501
PYT:D-SeV-Cl	4.07/111	4.08/364	4.04/284	4.07/759

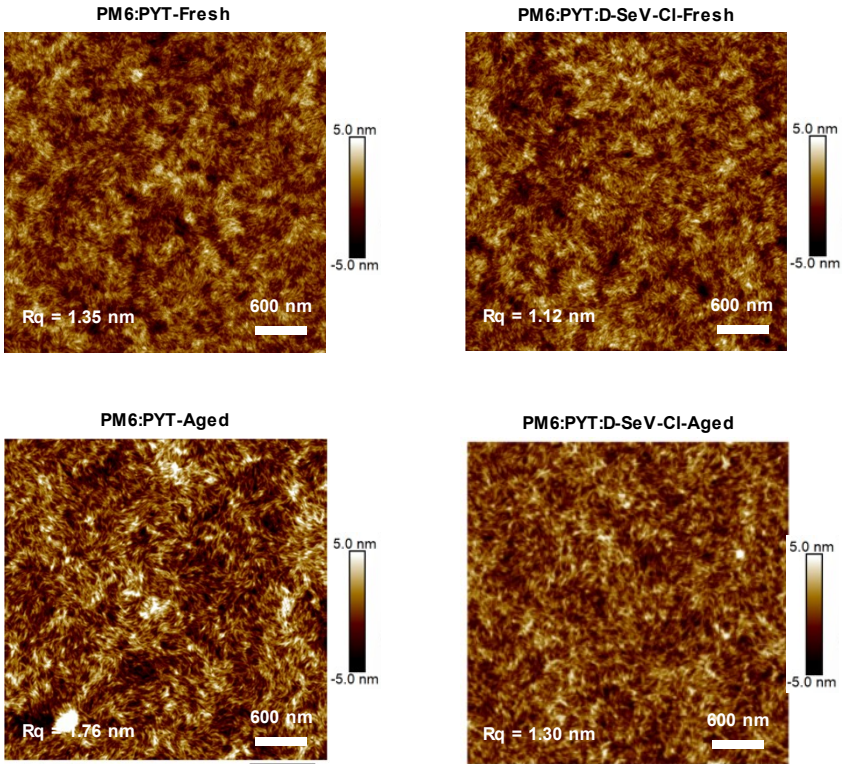

Figure S27. AFM images for the fresh and aged blend films of the PM6:PYT and PM6:PYT: D-SeV-Cl systems.

Table S8. Investigations of the morphology parameters extracted from the GIWAXS measurements of PM6:PYT, PM6:D-SeV-Cl and PM6:PYT:D-SeV-Cl active layers.

Systems	In plane		Out of plane			
	Lamellar stacking (100)		π-π stacking (010)			
	Q (Å^{-1})	*d* (Å)	*Q* (Å^{-1})	*d* (Å)	FWHM (Å^{-1})	CCL (Å)
PM6:PYT	0.294	21.36	1.639	3.83	0.320	19.62
PM6:D-SeV-Cl	0.308	20.38	1.628	3.85	0.289	21.73
PM6:PYT:D-SeV-Cl	0.296	21.22	1.649	3.81	0.280	22.43

Table S9. The packing distance (unit: Å) and number of different packing models of PYT in pristine PYT and blend PYT:D-SeV-Cl systems, and the packing distance and packing number of different packing models between PYT and D-SeV-Cl in blend PYT:D-SeV-Cl systems.

	Core-Core	Core-Terminal	Terminal-Terminal	Total
PYT (PYT)	4.09/111	4.07/337	4.04/243	4.06/691
PYT (PYT:D-SeV-Cl)	4.08/104	4.09/341	4.04/268	4.07/714
PYT-D-SeV-Cl (PYT:D-SeV-Cl)	3.97/7	4.04/23	4.17/15	4.04/45

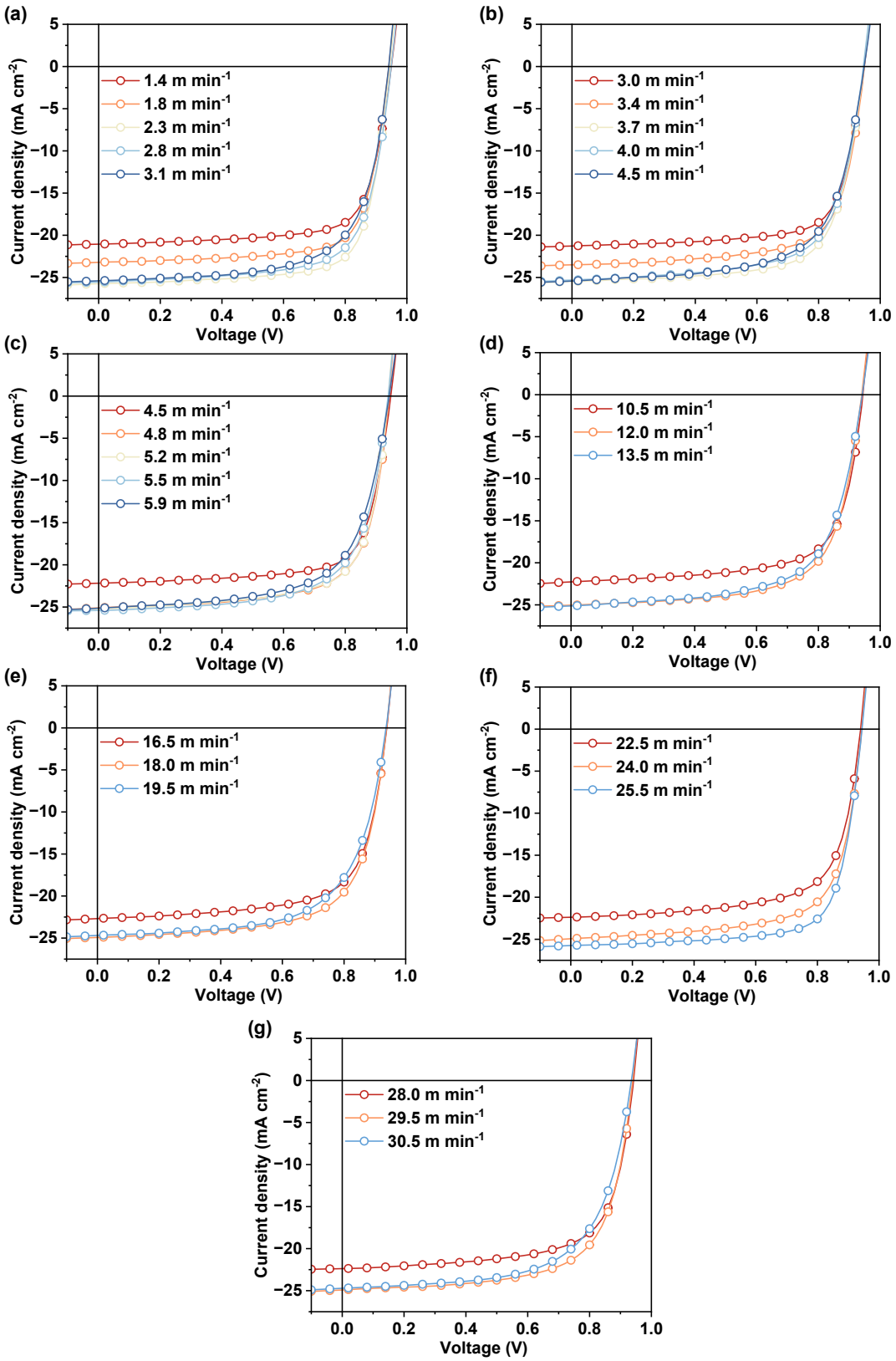

Figure S28. *J-V* curves of the PM6:PYT devices with different solution concentrations fabricated at different blade-coating speeds measured under one sun illumination.

Table S10. Photovoltaic parameters of the PM6:PYT devices fabricated at different blade-coating speeds.

Concentration [mg mL^{-1}]	Speed [m min^{-1}]	Thickness [nm]	V_{OC} [V]	J_{SC} [mA cm^{-2}]	FF [%]	PCE (Avg.[a]) [%]
16.0	1.4	62	0.949	21.05	74.47	14.93 (14.75±0.12)
	1.9	87	0.942	23.20	74.38	16.26 (16.02±0.12)
	2.3	110	0.944	25.20	74.29	18.06 (17.85±0.10)
	2.7	140	0.949	25.55	70.96	17.21 (17.00±0.18)
	3.1	158	0.941	25.39	67.90	16.23 (15.97±0.12)
14.0	3.0	74	0.947	21.27	73.30	14.76 (14.50±0.15)
	3.4	95	0.948	23.50	71.00	15.82 (15.55±0.18)
	3.7	108	0.947	25.46	70.62	17.02 (16.85±0.12)
	4.0	136	0.945	25.30	68.47	16.37 (16.10±0.20)
	4.5	152	0.947	25.42	66.11	15.91 (15.67±0.15)
12.0	4.5	80	0.947	22.18	72.38	15.20 (14.75±0.15)
	4.8	102	0.942	25.09	70.33	16.62 (16.40±0.12)
	5.2	125	0.940	25.23	70.37	16.69 (16.50±0.15)
	5.5	144	0.939	25.40	67.45	16.09 (15.80±0.18)
	5.9	158	0.942	25.14	65.58	15.53 (15.27±0.20)
10.0	10.5	91	0.943	22.27	70.02	14.71 (14.45±0.20)
	12.0	109	0.940	25.03	68.19	16.04 (16.02±0.12)
	13.5	132	0.941	25.12	65.89	15.57 (15.32±0.20)
8.0	16.5	88	0.939	22.68	69.30	14.75 (14.52±0.12)
	18.0	113	0.938	24.92	67.94	15.88 (15.75±0.10)

	19.5	134	0.936	24.69	64.80	14.98 (14.68±0.15)
	22.5	84	0.940	22.38	69.21	14.56 (14.35±0.18)
7.0	24.0	112	0.936	24.93	67.95	15.85 (15.62±0.12)
	25.5	138	0.935	24.80	64.79	14.92 (14.70±0.15)
	28.0	85	0.942	22.37	69.04	14.71 (14.55±0.12)
6.0	29.5	112	0.939	24.91	67.84	15.86 (15.54±0.12)
	30.5	136	0.935	24.71	64.27	14.85 (14.52±0.10)

[a]The values in brackets are the average PCE obtained from 10 devices.

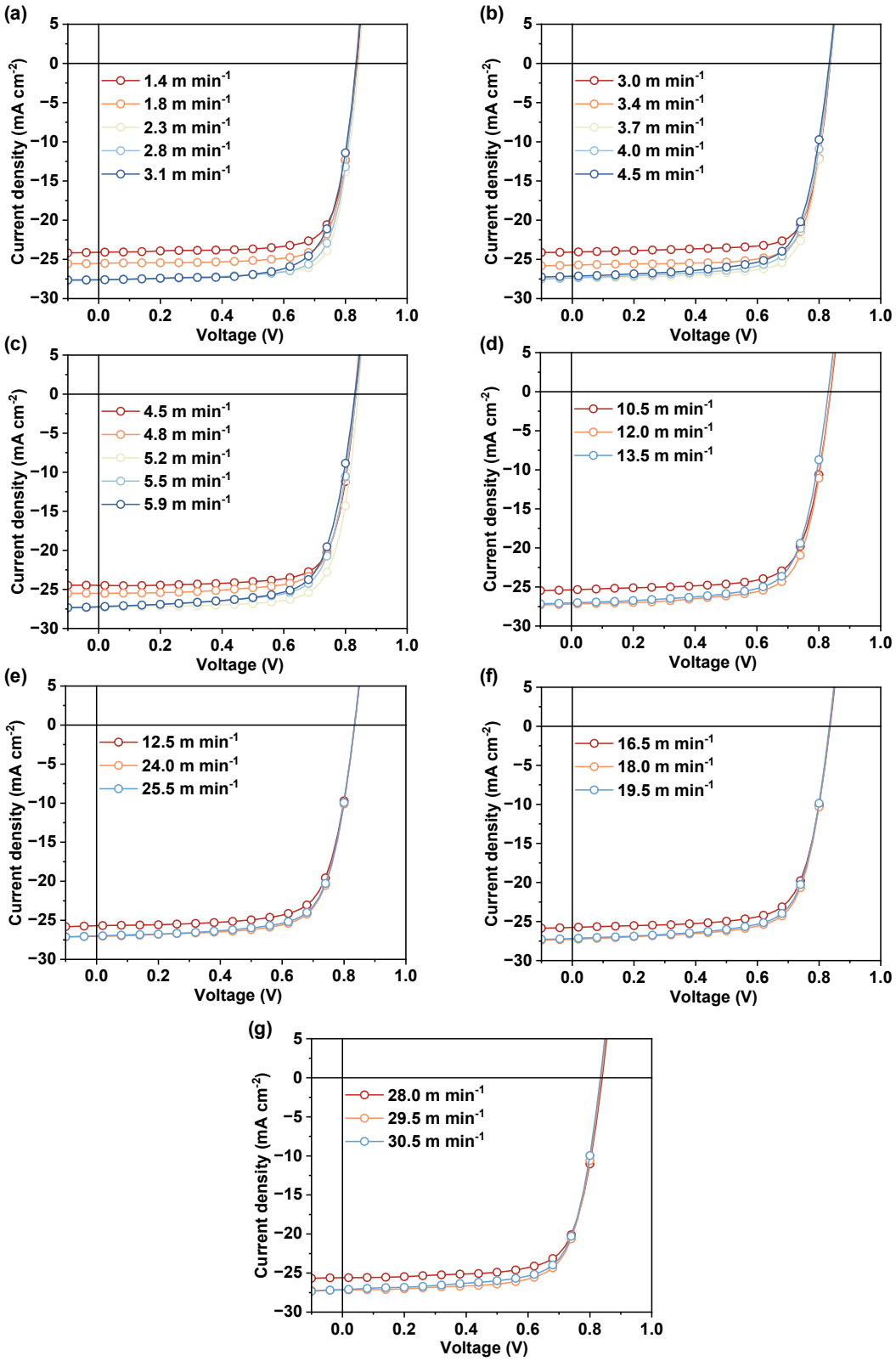

Figure S29. *J-V* curves of the PM6:D-SeV-Cl devices with different solution concentrations, fabricated at different blade-coating speeds, measured under one sun illumination.

Table S11. Photovoltaic parameters of the PM6:D-SeV-Cl devices fabricated at different blade-coating speeds.

Concentration [mg mL^{-1}]	Speed [m min^{-1}]	Thickness [nm]	V_{OC} [V]	J_{SC} [mA cm^{-2}]	FF [%]	PCE (Avg.[a]) [%]
16.0	1.4	68	0.837	24.09	77.21	15.56 (15.35±0.12)
	1.9	84	0.839	25.51	77.96	16.69 (16.52±0.10)
	2.3	110	0.843	27.64	77.32	18.01 (17.90±0.10)
	2.7	131	0.836	27.59	76.00	17.53 (17.27±0.18)
	3.1	155	0.835	27.60	72.47	16.70 (16.42±0.22)
14.0	3.0	70	0.837	24.07	77.39	15.59 (15.30±0.16)
	3.4	91	0.835	25.72	76.80	16.49 (16.25±0.20)
	3.7	108	0.834	27.34	76.45	17.43 (17.18±0.20)
	4.0	138	0.837	27.36	73.00	16.72 (16.40±0.22)
	4.5	154	0.834	27.14	72.05	16.31 (16.04±0.18)
12.0	4.5	70	0.835	24.48	76.35	15.61 (15.45±0.15)
	4.8	89	0.837	25.50	75.14	16.00 (15.70±0.15)
	5.2	110	0.840	27.33	75.57	17.38 (17.10±0.18)
	5.5	144	0.835	27.27	72.39	16.48 (16.20±0.20)
	5.9	158	0.832	27.21	71.43	16.17 (15.87±0.20)
10.0	10.5	91	0.838	25.37	73.35	15.59 (15.25±0.20)
	12.0	114	0.838	27.19	72.60	16.54 (16.32±0.18)
	13.5	136	0.834	27.04	71.57	16.14 (15.83±0.22)
8.0	16.5	92	0.836	25.75	73.06	15.72 (15.42±0.20)
	18.0	115	0.835	27.28	72.50	16.51 (16.36±0.10)

	19.5	133	0.834	27.16	71.99	16.30 (16.11±0.15)
7.0	22.5	90	0.834	25.69	73.07	15.65 (15.40±0.14)
	24.0	112	0.834	27.05	72.98	16.46 (16.28±0.14)
	25.5	140	0.832	27.00	71.90	16.15 (15.82±0.18)
6.0	28.0	90	0.838	25.59	73.30	15.71 (15.50±0.15)
	29.5	108	0.836	27.16	72.79	16.52 (16.40±0.18)
	30.5	136	0.834	27.11	71.57	16.18 (15.84±0.23)

[a]The values in brackets are the average PCE obtained from 10 devices.

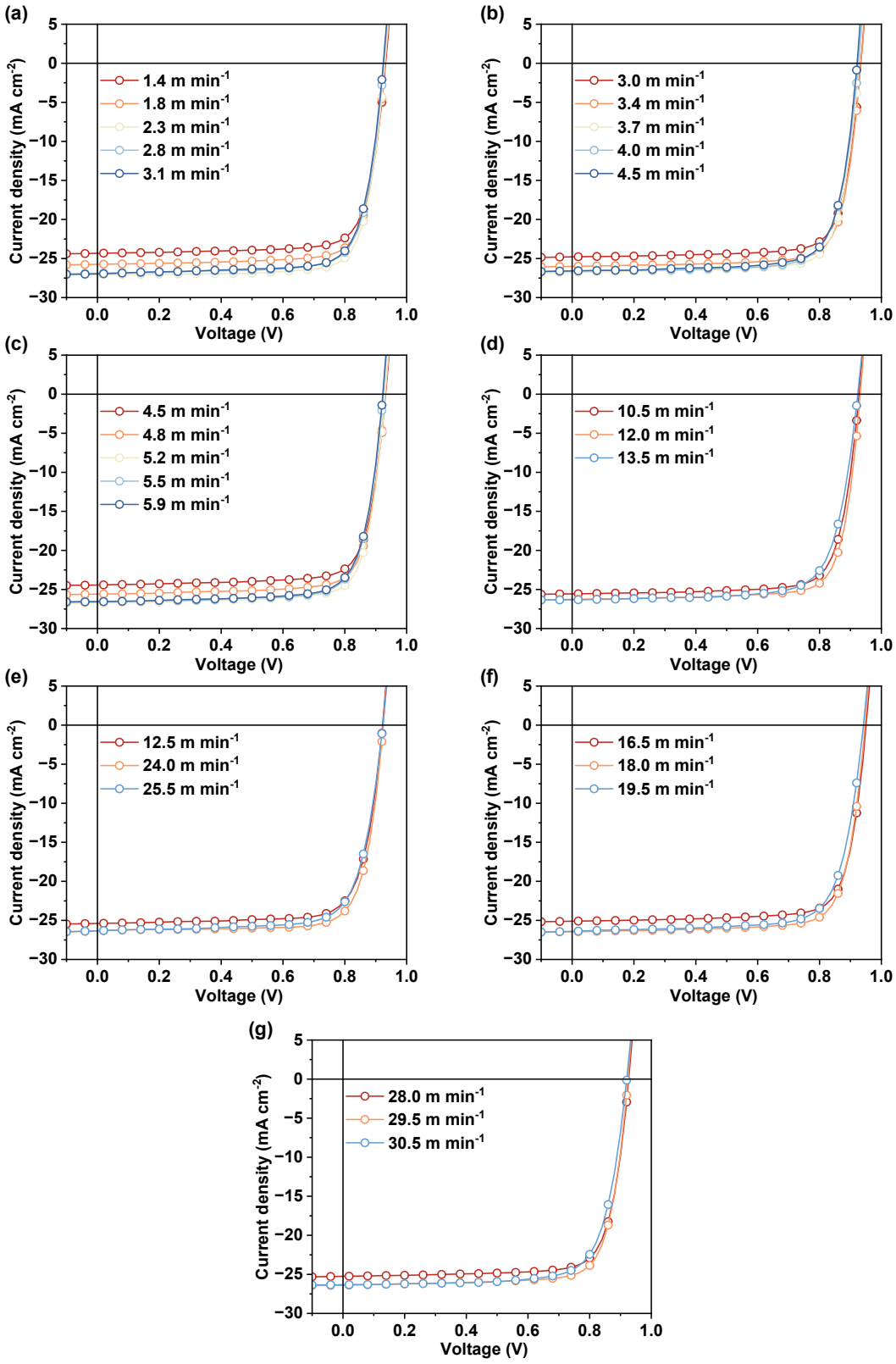

Figure S30. *J-V* curves of the PM6:PYT:D-SeV-Cl devices with different solution concentrations, fabricated at different blade-coating speeds measured under one sun illumination.

Table S12. Photovoltaic parameters of the PM6:PYT:D-SeV-Cl devices fabricated at different blade-coating speeds.

Concentration [mg mL^{-1}]	Speed [m min^{-1}]	Thickness [nm]	V_{OC} [V]	J_{SC} [mA cm^{-2}]	FF [%]	PCE (Avg.[a]) [%]
16.0	1.4	74	0.931	24.33	78.70	17.83 (17.45±0.12)
	1.9	90	0.930	25.74	78.72	18.84 (18.52±0.12)
	2.3	113	0.932	27.15	79.11	20.01 (19.70±0.20)
	2.7	126	0.926	26.87	77.62	19.31 (19.04±0.18)
	3.1	138	0.925	26.97	77.16	19.25 (18.84±0.12)
14.0	3.0	80	0.933	24.78	78.79	18.22 (17.92±0.16)
	3.4	94	0.933	26.00	78.99	19.16 (18.80±0.18)
	3.7	114	0.928	26.79	78.52	19.52 (19.22±0.20)
	4.0	130	0.925	26.58	77.01	18.93 (18.65±0.15)
	4.5	142	0.925	26.59	76.86	18.90 (18.47±0.25)
12.0	4.5	79	0.931	24.43	78.41	17.84 (17.45±0.14)
	4.8	100	0.930	25.60	78.55	18.70 (18.40±0.12)
	5.2	116	0.926	26.75	77.94	19.31 (19.02±0.12)
	5.5	130	0.925	26.50	77.33	18.96 (18.68±0.16)
	5.9	144	0.925	26.58	76.74	18.87 (18.55±0.12)
10.0	10.5	94	0.928	25.56	78.10	18.52 (18.22±0.14)
	12.0	110	0.930	26.26	78.89	19.26 (18.94±0.15)
	13.5	130	0.924	26.32	75.25	18.30 (17.95±0.20)
8.0	16.5	90	0.923	25.38	77.20	18.08 (17.76±0.15)
	18.0	108	0.924	26.34	78.24	19.04 (18.90±0.10)

	19.5	127	0.924	26.36	75.56	18.40 (18.22±0.14)
7.0	22.5	90	0.93	25.10	78.63	18.35 (18.08±0.16)
	24.0	112	0.926	26.45	78.10	19.13 (18.93±0.14)
	25.5	130	0.924	26.41	75.24	18.35 (18.10±0.10)
6.0	28.0	88	0.926	25.25	78.16	18.27 (17.95±0.10)
	29.5	115	0.925	26.40	78.00	19.05 (18.84±0.15)
	30.5	130	0.921	26.336	74.80	18.14 (17.88±0.12)

[a]The values in brackets are the average PCE obtained from 10 devices.

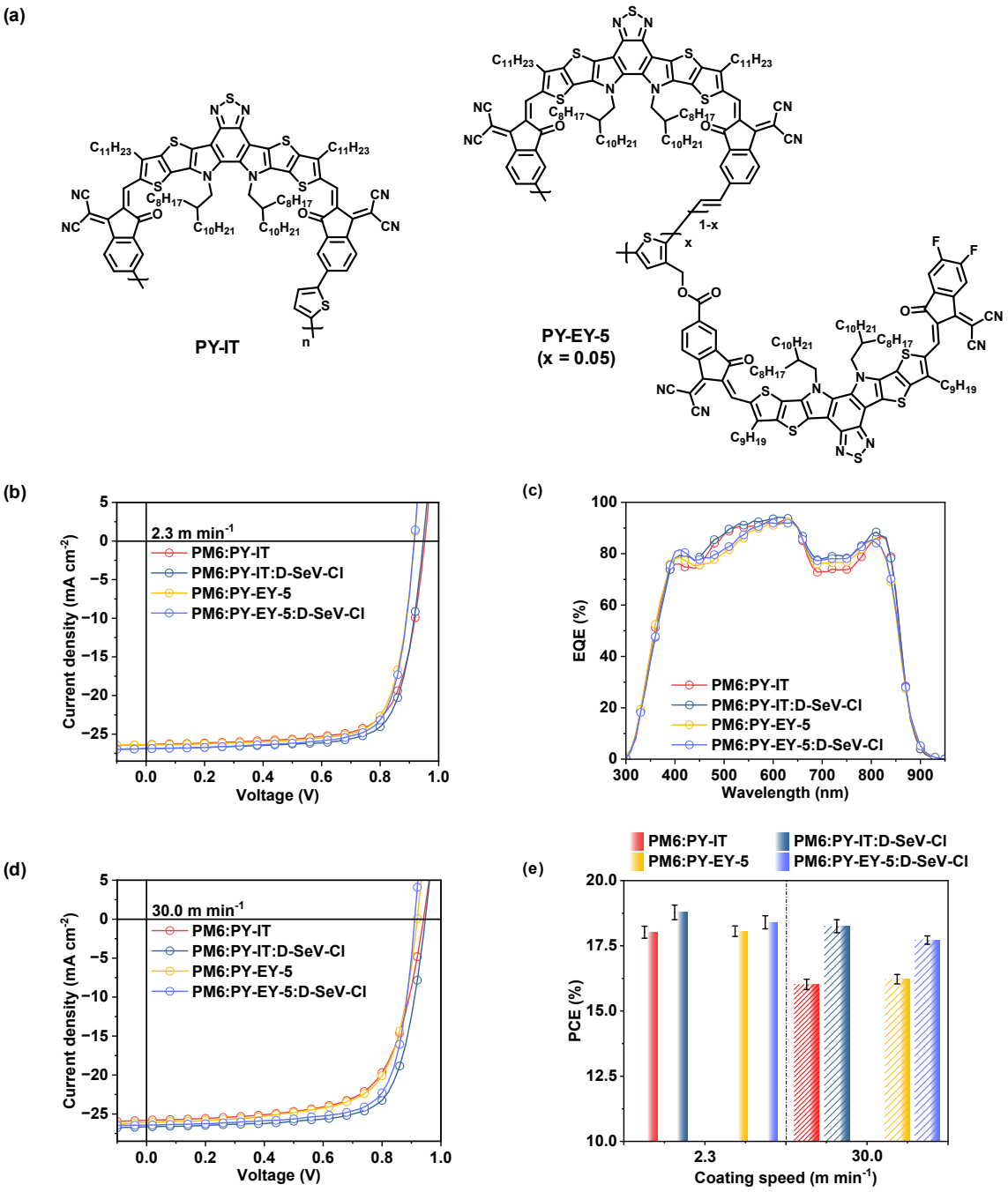

Figure S31. (a) The chemical structure of PY-IT and PY-EY-5. (b) The *J-V* curves of the PM6:PY-IT and PM6:PY-EY-5 treated with D-SeV-Cl devices fabricated with a speed of 2.3 m min^{-1}. (c) The EQE curves of relevant devices. (d) The *J-V* curves of the PM6:PY-IT and PM6:PY-EY-5 treated with D-SeV-Cl devices fabricated with a speed of 30.0 m min^{-1}. (e) The summarized PCEs extracted from 2.3 m min^{-1} and 30.0 m min^{-1} from the PM6:PY-IT and PM6:PY-EY-5 systems.

Table S13. Photovoltaic parameters of the devices of PM6:PY-IT and PM6:PY-EY-5 systems fabricated under 2.3 m min^{-1} and 30.0 m min^{-1} measured under one sun illumination.

Active layer	Speed [m min^{-1}]	V_{OC} [V]	J_{SC} [mA cm^{-2}]	$J_{SC\ cal}$ [mA cm^{-2}]	FF [%]	PCE (Avg.[a]) [%]
PM6:PY-IT	2.3	0.952	26.36	25.81	73.01	18.32 (18.02±0.23)
PM6:PY-IT:D-SeV-Cl		0.947	26.88	26.50	75.30	19.16 (18.78±0.28)
PM6:PY-EY-5		0.917	26.38	25.75	75.40	18.24 (18.06±0.20)
PM6:PY-EY-5:D-SeV-Cl		0.916	26.88	25.82	75.55	18.60 (18.40±0.25)
PM6:PY-IT	30.0	0.941	25.81	/	67.01	16.27 (16.02±0.20)
PM6:PY-IT:D-SeV-Cl		0.946	26.65	/	73.47	18.52 (18.25±0.25)
PM6:PY-EY-5		0.919	26.11	/	69.10	16.58 (16.22±0.18)
PM6:PY-EY-5:D-SeV-Cl		0.910	26.41	/	74.60	17.92 (17.72±0.16)

[a]The values in brackets are the average PCE obtained from 10 devices.

Table S14. Photovoltaic parameters of the large devices and modules of PM6:PYT, PM6:D-SeV-Cl and PM6:PYT:D-SeV-Cl systems measured under one sun illumination.

Active layer	Area [cm^2]	V_{OC} [V]	J_{SC} [mA cm^{-2}]	FF [%]	PCE (Avg.[a]) [%]
PM6:PYT	1.0	0.943	25.09	70.35	16.64 (16.28±0.25)
	15.4	7.528	3.11	64.98	15.21 (14.90±0.18)
PM6:D-SeV-Cl	1.0	0.846	26.68	73.61	16.61 (16.40±0.22)
	15.4	6.739	3.32	66.55	14.89 (14.65±0.20)
PM6:PYT:D-SeV-Cl	1.0	0.930	26.47	77.31	19.03 (18.56±0.15)
	15.4	7.440	3.20	71.25	16.96 (16.75±0.18)

[a]The values in brackets are the average PCE obtained from 10 devices.

References

1. H. Fu, Q. Fan, W. Gao, J. Oh, Y. Li, F. Lin, F. Qi, C. Yang, T. J. Marks, A. K. Y. Jen, *Sci. China Chem.*, **2021**, *65*, 309.
2. M. J. Abraham, T. Murtola, R. Schulz, S. Páll, J. C. Smith, B. Hess, E. Lindahl, *SoftwareX*, **2015**, *1-2*, 19.
3. J. Wang, R. M. Wolf, J. W. Caldwell, P. A. Kollman, D. A. Case, *J. Comput. Chem.*, **2004**, *25*, 1157.
4. B. Hess, H. Bekker, H. J. C. Berendsen, J. G. E. M. Fraaije, *J. Comput. Chem.*, **1997**, *18*, 1463.
5. M. Parrinello,A. Rahman, *J. Appl. Phys.*, **1981**, *52*, 7182.
6. G. Bussi, D. Donadio, M. Parrinello, *J Chem Phys*, **2007**, *126*, 014101.
7. U. Essmann, L. Perera, M. L. Berkowitz, T. Darden, H. Lee, L. G. Pedersen, *J. Chem. Phys.*, **1995**, *103*, 8577.
8. A. D. William Humphrey, Klaus Schulten, *J. Mol. Graph.* , **1996**, *14*, 33.
9. X. Gu, Y. Zhou, K. Gu, T. Kurosawa, Y. Guo, Y. Li, H. Lin, B. C. Schroeder, H. Yan, F. Molina-Lopez, C. J. Tassone, C. Wang, S. C. B. Mannsfeld, H. Yan, D. Zhao, M. F. Toney and Z. Bao, *Adv. Energy Mater.*, **2017**, *7*, 1602742.
10. L. Zhu, W. Zhong, C. Qiu, B. Lyu, Z. Zhou, M. Zhang, J. Song, J. Xu, J. Wang, J. Ali, W. Feng, Z. Shi, X. Gu, L. Ying, Y. Zhang and F. Liu, *Adv. Mater.*, **2019**, *31*, 1902899.
11. S. A. Schneider, K. L. Gu, H. Yan, M. Abdelsamie, Z. Bao and M. F. Toney, *Chem. Mater.*, **2021**, *33*, 5951-5961.
12. Q. Wu, W. Wang, Y. Wu, Z. Chen, J. Guo, R. Sun, J. Guo, Y. Yang and J. Min, *Adv. Funct. Mater.*, **2021**, *31*, 2010411.
13. Y. Zhang, N. Wang, Y. Wang, J. Zhang, J. Liu and L. Wang, *iScience*, **2021**, *24*, 103104.
14. H. Yu, M. Pan, R. Sun, I. Agunawela, J. Zhang, Y. Li, Z. Qi, H. Han, X. Zou, W. Zhou, S. Chen, J. Y. L. Lai, S. Luo, Z. Luo, D. Zhao, X. Lu, H. Ade, F. Huang, J. Min and H. Yan, *Angew. Chem. Int. Ed.*, **2021**, *60*, 10137-10146.
15. D. Chen, S. Liu, B. Huang, J. Oh, F. Wu, J. Liu, C. Yang, L. Chen and Y. Chen, *Small*, **2022**, *18*, 2200734.

16. D. Chen, S. Liu, X. Hu, F. Wu, J. Liu, K. Zhou, L. Ye, L. Chen and Y. Chen, *Sci. China Chem.*, **2021**, *65*, 182-189.
17. Y.-Z. Zhang, N. Wang, Y.-H. Wang, J.-H. Miao, J. Liu and L.-X. Wang, *Chinese J. Polym. Sci*., **2022**, *40*, 989-995.
18. J. Liu, J. Liu, J. Deng, B. Huang, J. Oh, L. Zhao, L. Liu, C. Yang, D. Chen, F. Wu and L. Chen, *J. Energy Chem.*, **2022**, *71*, 631-638.
19. Y. Yue, B. Zheng, W. Yang, L. Huo, J. Wang and L. Jiang, *Adv. Mater*., **2022**, *34*, 2108508.
20. A. Harillo-Baños, Q. Fan, S. Riera-Galindo, E. Wang, O. Inganäs and M. Campoy-Quiles, *ChemSusChem*, **2022**, *15*, e202101888.
21. N. Yao, Q. Fan, Z. Genene, H. Liu, Y. Xia, G. Wen, Y. Yuan, E. Moons, J. van Stam, W. Zhang, X. Lu, E. Wang and F. Zhang, *Sol. RRL*, **2023**, *7*, 2201134.
22. B. Shi, Y. Li, J. Sun, R. Sun, D. Jiang, R. Zhou, R. Zhang, J. Qiao, S. H. Pun, J. Yi, X. Xia, P. Lu, Y. Wang, G. Zhang, T. He, M. Zhang, Z. Ji, X. Du, J. Min, F. Chen, F. Gao, X. Hao, H. Yan and H. Yin, *Adv. Mater.*, **2025**, DOI: 10.1002/adma.202505313, e05311.
23. X. Wu, B. Xiao, R. Sun, X. Yang, M. Zhang, Y. Gao, B. Xiao, E. D. Papkovskaya, Y. Luponosov, C. J. Brabec and J. Min, *Energy Environ. Sci.*, **2025**, *18*, 1812–1823.